INTERNATIONAL JOURNAL FOR NUMERICAL METHODS IN FLUIDS
Int. J. Numer. Meth. Fluids 2001; **35**: 449–494

A Boltzmann based model for open channel flows

M. S. Ghidaoui[a,*], J. Q. Deng[a], W. G. Gray[b] and K. Xu[c]

[a] *Department of Civil Engineering, The Hong Kong University of Science and Technology, Kowloon, Hong Kong*
[b] *Center for Water Research, The University of Western Australia, Nedlands, Western Australia*
[c] *Department of Mathematics, The Hong Kong University of Science and Technology, Kowloon, Hong Kong*

SUMMARY

A finite volume, Boltzmann Bhatnagar–Gross–Krook (BGK) numerical model for one- and two-dimensional unsteady open channel flows is formulated and applied. The BGK scheme satisfies the entropy condition and thus prevents unphysical shocks. In addition, the van Leer limiter and the collision term ensure that the BGK scheme admits oscillation-free solutions only. The accuracy and efficiency of the BGK scheme are demonstrated through the following examples: (i) strong shock waves, (ii) extreme expansion waves, (iii) a combination of strong shock waves and extreme expansion waves, and (iv) one- and two-dimensional dam break problems. These test cases are performed for a variety of Courant numbers (C_r), with the only condition being $C_r \leq 1$. All the computational results are free of spurious oscillations and unphysical shocks (i.e., expansion shocks). In addition, comparisons of numerical tests with measured data from dam break laboratory experiments show good agreement for $C_r \leq 0.6$. This reduction in the stability domain is due to the explicit integration of the friction term. Furthermore, BGK schemes are easily extended to multidimensional problems and do not require characteristic decomposition. The proposed scheme is second-order in both space and time when the external forces are zero and second-order in space but first-order in time when the external forces are non-zero. However, since all the test cases presented are either for zero or small values of external forces, the results tend to maintain second-order accuracy. In problems where the external forces become significant, it is possible to improve the order of accuracy of the scheme in time by, for example, applying the Runge–Kutta method in the integration of the external forces. Copyright © 2001 John Wiley & Sons, Ltd.

KEY WORDS: Boltzmann equation; bore entropy; dam break; numerical model; unsteady open channel flow

1. INTRODUCTION

Modeling of problems in mechanics, hydrodynamics, hydraulics, and environmental fluid mechanics may be undertaken at three different length scales, commonly referred to as the microscopic, mesoscopic, and macroscopic levels [1]. Microscopic modeling involves the

* Correspondence to: Department of Civil Engineering, The Hong Kong University of Science and Technology, Kowloon, Hong Kong.

Received 2 June 1999
Revised 25 April 2000

application of Newton's laws to every molecule in the system. It requires knowledge of the initial state of each molecule and the quantification of the interactions among all the molecules in the system. Because of the level of detail needed, microscopic modeling is computationally infeasible except in some cases where the mean free path between molecules is large. Mesoscopic modeling (i.e., modeling from statistical perspectives) entails the application of Newton's laws to a probability distribution of molecules. Mesoscopic modeling uses the Boltzmann equation as a starting point for system simulation, where the dependent variable is the probability distribution of particles [2]. Mass, momentum, energy, and entropy are computed from the moments of this distribution function. Macroscopic modeling entails the application of the basic laws of mechanics and thermodynamics to a continuum. Examples of the macroscopic continuum models in hydraulic engineering, hydrodynamics, and environment fluid mechanics include shallow water (i.e., Saint-Venant) equations, water hammer equations, Richard's unsaturated flow equation, Navier–Stokes equations, and the equation of chemical species transport.

Until recently, the analyses and solutions of problems in hydraulics, hydrodynamics, and environmental fluid mechanics have been based exclusively on macroscopic continuum models, which are solved either analytically or numerically. However, over the last three decades numerical schemes based on mesoscopic models have been developed and applied to a multitude of hydrodynamic problems, including shock waves in compressible flows [2–5], multicomponent and multiphase flows [6–8], flows in complex geometries [9,10], turbulent flows [11,12], low Mach number flows [13], and heat transfer and reaction diffusion flows [14,15]. Two sub-classes of mesoscopic models have emerged: lattice Boltzmann (LB) models and the continuous Boltzmann Bhatnagar–Gross–Krook (BKG) models. The distribution function in LB models is discrete in particle velocity [1]. However, the distribution function in BGK models is continuous in particle velocity [13]. Excellent reviews of the LB models and BGK models are provided in References [10,15] respectively.

The main advantages of mesoscopic LB or BGK based numerical models over macroscopic based numerical models are summarized below

1. While the advective operator in the macroscopic approach is non-linear, its counterpart in the mesoscopic approach is linear [10].
2. A mesoscopic based numerical model can be easily extended to multidimensional flows because the distribution function of particles is a scalar [5].
3. In mesoscopic modeling, the implementation of complex boundary conditions is straightforward [1,2,10,16].
4. In mesoscopic modeling, the incompressible flow solution is obtained in the limit as Mach number tends to zero. This means that the solution of two- and three-dimensional non-hydrostatic surface water models do not involve the tedious and difficult solution of the Poisson equation for the pressure field [13].
5. The scalar nature of the Boltzmann distribution and the fact that the Boltzmann equation is only a first-order ordinary differential equation (ODE) means that mesoscopic modeling possesses the intrinsic features required for parallel computation [10,16]. This is highly beneficial for direct numerical simulation (DNS) and large eddy simulation (LES) of turbulent open channel flows.

6. The diffusion and viscous terms that appear as second derivative terms in macroscopic modeling are represented by a simple algebraic difference term in mesoscopic modeling. Thus, the need for separate treatment of the advection and diffusion terms is eliminated.
7. The collision function in mesoscopic models eliminates the need for numerical entropy fixes to ensure that the second law of thermodynamics is not violated by the solution [4]. In contrast, macroscopic numerical models require *ad hoc* entropy fixes in order to satisfy the entropy condition [2,4].

The fact that mesoscopic numerical models satisfy the entropy condition was exploited in References [4,17] to model shock waves in compressible flows and in References [6–8,18] to model interfaces in multiphase and multicomponent flows. These applications revealed that the mesoscopic approach (i) accurately resolves shocks an discontinuities and (ii) does not suffer from the failures associated with the Riemann solution of macroscopic hydrodynamics equations. The failures of Riemann solvers are well documented in References [19–21] and will not be discussed in this paper.

The many attributes of mesoscopic modeling, particularly its success in resolving shocks in compressible flows and resolving interfacial discontinuities in multiphase flow, suggest that this method may be useful in simulating open channel flows, where hydraulic jumps may occur. In the present paper, the collisional BGK model is formulated and applied to one- and two-dimensional shallow water flows. Numerical experiments show that the BGK based shallow water model produces highly accurate results for rapidly and gradually varied open channel flow problems and does not suffer from aphysical oscillations as encountered when applying Riemann solvers to the macroscopic equations. This finding is consistent with conclusions reported by researchers using Boltzmann theory to model shock waves in compressible flows [2,4,5,22,23]. Moreover, mesoscopic based numerical models are simpler to formulate, apply, and code than Riemann solver models since they do not require characteristic decomposition.

This paper is organized as follows. First, the fundamentals of kinetic theory and the two-dimensional Boltzmann equation for open channel flow are introduced and discussed. Second, the relation between the two-dimensional Boltzmann equation and the macroscopic shallow water equation is established. Third, the numerical solution of the two-dimensional Boltzmann equation for open channel flow is formulated. Fourth, the Boltzmann-based numerical model is applied to a range of open channel flow problems and the results are discussed. Last, the findings of the paper are summarized.

2. THE BOLTZMANN EQUATION FOR TWO-DIMENSIONAL OPEN CHANNEL FLOWS

The two-dimensional collisional BGK Boltzmann equation can be written as follows [4,8,24,25]:

$$\frac{\partial f}{\partial t} + \mathbf{c}\cdot\nabla f + \frac{\mathbf{F}}{m}\cdot\frac{\partial f}{\partial \mathbf{c}} = \frac{h-f}{\tau} \tag{1}$$

where f is the irreversible (non-equilibrium) particle distribution; h is the reversible (equilibrium) distribution of particles; t is time; ∇ is the two-dimensional spatial derivative operator with respect to x and z, the Cartesian co-ordinates; m is the mass of a particle; $\mathbf{c}$ is the particle velocity vector with components c_x and c_z in the x- and z-directions respectively; $\mathbf{F}$ is the net external force acting on the particles with components F_x and F_z; and τ is the collision (or relaxation) time, which is a measure of the average time a particle spends between consecutive collisions. With the channel slopes in the x- and z-directions assumed to be small, the net external force is [26]

$$\frac{\mathbf{F}}{m} = g(\mathbf{S}_0 - \mathbf{S}_\mathrm{f}) \tag{2}$$

where $\mathbf{S}_0$ is the channel slope vector and $\mathbf{S}_\mathrm{f}$ is the friction slope. Of course, other external forces such as wind stresses can be added. The details of the collision time τ, which depends on the macroscopic flow variable, will be discussed in the numerical description section. Note that the right-hand side of Equation (1) is a measure of the deviation of the non-equilibrium from the equilibrium distribution. According to Equation (1), the collision term $(h-f)/\tau$ drives the non-equilibrium distribution f towards equilibrium state h. The flow reaches local equilibrium when $f = h$ and $\mathrm{d}h/\mathrm{d}t = 0$ such that the collision term is non-varying and equal to zero [27].

2.1. Basic relationships between macroscopic and mesoscopic properties

The Primary macroscopic quantities that characterize the flow of water in a channel are $\rho \equiv$ density, $y(\mathbf{x}, t) \equiv$ fluid depth, $\mathbf{v}(\mathbf{x}, t) \equiv$ fluid velocity with components u and v in the x- and z-directions respectively, $\mathbf{T}(\mathbf{x}, t) \equiv$ stress tensor, and $S(\mathbf{x}, t) \equiv$ entropy. The fundamental relationships among these macroscopic quantities and the mesoscopic properties f and $\mathbf{c}$ are as follows [25]:

$$y = \int_{-\infty}^{\infty}\int_{-\infty}^{\infty} f \,\mathrm{d}c_x \,\mathrm{d}c_z \tag{3}$$

$$y\mathbf{v} = \int_{-\infty}^{\infty}\int_{-\infty}^{\infty} \mathbf{c}f \,\mathrm{d}c_x \,\mathrm{d}c_z \tag{4}$$

$$y\left[\mathbf{vv} - \frac{1}{\rho}\mathbf{T}\right] = \int_{-\infty}^{\infty}\int_{-\infty}^{\infty} \mathbf{cc}f \,\mathrm{d}c_x \,\mathrm{d}c_z \tag{5}$$

$$S = -\int_{-\infty}^{\infty}\int_{-\infty}^{\infty} f \ln(Af) \,\mathrm{d}c_x \,\mathrm{d}c_z \tag{6}$$

where A is a normalizing coefficient that will be determined subsequently. The macroscopic variables in the above equations all depend on $(\mathbf{x}, t)$. Also, since integration is performed over the particle velocities, these equations may be divided by the depth y, which may be moved into the integrands. Essentially, relationships (3)–(6) form the bridge between the macroscopic

properties and the mesoscopic properties of a substance and, thereby, link the classical laws of mechanics with the Boltzmann equation of kinetic theory.

From a statistical mechanics perspective, f/y is the joint probability distribution of the random particle velocity variable $\mathbf{c}$. The integral of f/y over all particle speeds is equal to 1. Therefore, $\mathbf{v}$ is the mean particle velocity. In addition, the off-diagonal elements of $\mathbf{T}$ are the conditional variances in c_x given c_z as well as the conditional variance in c_z given c_x. This is equivalent to stating that the pressure is unique at a point. Furthermore, the non-equilibrium part of $\mathbf{T}$ (i.e., the shear stress) is the covariance of the distribution f/y. In fact, Vincenti and Kruger [27] have shown that when a flow reaches local equilibrium (i.e., $f = h$), the covariance of h/y and thus the shear stresses are zero. For our system, this implies the following equilibrium identity:

$$\frac{p}{\rho}\mathbf{I} = \int_{-\infty}^{\infty}\int_{-\infty}^{\infty}(\mathbf{c}-\mathbf{v})(\mathbf{c}-\mathbf{v})\frac{h}{y}\,\mathrm{d}c_x\,\mathrm{d}c_z \tag{7}$$

Indeed for our set of equations the viscous terms will be neglected and Equation (7) will be enforced as well, with h replaced by f.

The fundamental laws of classical physics dictate that mass, momentum, and energy of particles are collision invariant [25]. As a consequence, the following compatibility conditions hold:

$$\int_{-\infty}^{\infty}\int_{-\infty}^{\infty}\frac{h-f}{\tau}\,\mathrm{d}c_x\,\mathrm{d}c_z = 0 \tag{8}$$

$$\int_{-\infty}^{\infty}\int_{-\infty}^{\infty}\mathbf{c}\frac{h-f}{\tau}\,\mathrm{d}c_x\,\mathrm{d}c_z = \mathbf{0} \tag{9}$$

$$\int_{-\infty}^{\infty}\int_{-\infty}^{\infty}\mathbf{cc}\frac{h-f}{\tau}\,\mathrm{d}c_x\,\mathrm{d}c_z = \mathbf{0} \tag{10}$$

2.2. Derivation of the equilibrium distribution function h

Boltzmann (1872) defined a function $H = -S$ and showed that H monotonically decreases with time, reaching its minimum value at equilibrium (i.e., when $f = h$). The H theorem may be stated mathematically as

$$\frac{\mathrm{d}H}{\mathrm{d}t} \le 0 \text{ for all } f \text{ and } \delta H = 0 \text{ when } h = f \tag{11}$$

where δH indicates a variation in the value of H. Since $H = -S$, the H theorem in terms of S is

$$\frac{\mathrm{d}S}{\mathrm{d}t} \ge 0 \text{ for all } f \text{ and } \delta S = 0 \text{ when } h = f \tag{12}$$

That is, S monotonically increases with time and attains its maximum value at the equilibrium state, $f = h$.

For our problem, the maximization of S must be performed subject to definitions (3)–(5). These definitions may be applied as constraints on definition (6) using Lagrange multipliers to obtain

$$S = -\int_{-\infty}^{\infty}\int_{-\infty}^{\infty}[f\ln(Af) + \lambda_0 f + \boldsymbol{\lambda}\cdot\mathbf{c}f + \boldsymbol{\Lambda}\colon(\mathbf{c}-\mathbf{v})(\mathbf{c}-\mathbf{v})f]\,\mathrm{d}c_x\,\mathrm{d}c_z + \lambda_0 y + \boldsymbol{\lambda}\cdot\mathbf{v}y + \boldsymbol{\Lambda}\colon\mathbf{I}\frac{py}{\rho} \tag{13}$$

where λ_0, $\boldsymbol{\lambda}$, and $\boldsymbol{\Lambda}$ are the Lagrange multipliers that will be determined by analyzing a variation of Equation (13) around the equilibrium state. Note immediately that because the off diagonal elements of $\boldsymbol{\Lambda}$ cannot contribute to the entropy generation, they must be zero such that $\boldsymbol{\Lambda}$ is a diagonal tensor. Before applying the H theorem to the open channel flow problem, assume that the pressure distribution is hydrostatic such that the average pressure is given by $p = \rho g y/2$, where g is the gravitational acceleration. Then take the variation of S as given by Equation (13) with respect to f, y, u, and v for fixed t, $\mathbf{x}$, and $\mathbf{c}$ while holding the Lagrange multipliers constant. This gives

$$\delta S = -\int_{-\infty}^{\infty}\int_{-\infty}^{\infty}\delta f[\ln(Af) + 1 + \lambda_0 + \boldsymbol{\lambda}\cdot\mathbf{c} + \boldsymbol{\Lambda}\colon(\mathbf{c}-\mathbf{v})(\mathbf{c}-\mathbf{v})]\,\mathrm{d}c_x\,\mathrm{d}c_z + \delta y[\lambda_0 + \boldsymbol{\lambda}\cdot\mathbf{v} + \boldsymbol{\Lambda}\colon\mathbf{I}gy] + \delta\mathbf{v}\cdot\boldsymbol{\lambda}y \tag{14}$$

The H theorem, as given by Equation (12), indicates that at equilibrium the entropy will be a maximum such that a variation of entropy at the equilibrium state will provide $\delta S = 0$. For this condition to hold, the coefficients of each of the independent variations in Equation (14) must be zero. With $f = h$ at equilibrium, the conditions for equilibrium are

$$\ln(Ah) + 1 + \lambda_0 + \boldsymbol{\lambda}\cdot\mathbf{c} + \boldsymbol{\Lambda}\colon(\mathbf{c}-\mathbf{v})(\mathbf{c}-\mathbf{v}) = 0 \tag{15}$$

$$\lambda_0 + \boldsymbol{\lambda}\cdot\mathbf{v} + \boldsymbol{\Lambda}\colon\mathbf{I}gy = 0 \tag{16}$$

$$\boldsymbol{\lambda}y = 0 \tag{17}$$

Solution of Equation (15) for h subject to the restriction enforced by Equation (17) that $\boldsymbol{\lambda} = 0$ and the condition that the off-diagonal elements of $\boldsymbol{\Lambda}$ are 0 gives

$$h = \frac{1}{A}\exp[-1-\lambda_0]\exp[-\boldsymbol{\Lambda}\colon(\mathbf{c}-\mathbf{v})(\mathbf{c}-\mathbf{v})] \tag{18}$$

which is a two-dimensional Gaussian distribution.

Inserting the form of h given by Equation (18) into the right-hand side of definitions (3)–(5) at equilibrium and carrying out the integration produces a system of five equations for Lagrange multipliers

$$y = \frac{1}{A}\,\mathrm{e}^{-1-\lambda_0}\,\frac{\pi}{(\Lambda_{11}\Lambda_{22})^{1/2}}\exp(\boldsymbol{\Lambda}\colon\ \mathbf{vv}) \tag{19}$$

$$y\mathbf{v} = \mathbf{v}\,\frac{1}{A}\,\mathrm{e}^{-1-\lambda_0}\,\frac{\pi}{(\Lambda_{11}\Lambda_{22})^{1/2}}\exp(\boldsymbol{\Lambda}\colon\ \mathbf{vv}) \tag{20}$$

$$y\left(\mathbf{vv} + \frac{gy}{2}\,\mathbf{I}\right) = \left(\mathbf{vv} + \frac{1}{2}\,\Lambda^{-1}\right)\frac{1}{A}\,\mathrm{e}^{-1-\lambda_0}\,\frac{\pi}{(\Lambda_{11}\Lambda_{22})^{1/2}}\exp(\Lambda\colon\ \mathbf{vv}) \tag{21}$$

These equations are consistent with Equations (16) and (17) and may be solved algebraically for Lagrange multipliers. For example, division of Equation (21) by y as defined by Equation (19) readily shows that

$$\Lambda_{11} = \Lambda_{22} = \frac{1}{gy} \tag{22}$$

Insertion of these coefficients into Equation (19) gives

$$\frac{1}{A}\exp(-1-\lambda_0) = \frac{1}{\pi g}\exp\left[-\frac{\mathbf{v}\cdot\mathbf{v}}{gy}\right] \tag{23}$$

Equation (16) may be employed with this expression to obtain separate expressions for A and λ_0 as

$$A = e\pi g \tag{24}$$

$$\lambda_0 = -2 + \frac{\mathbf{v}\cdot\mathbf{v}}{gy} \tag{25}$$

Finally, the values for A and the Lagrange multipliers may be substituted into Equation (18) to provide the equilibrium distribution function

$$h(\mathbf{x}, \mathbf{c}, t)\frac{1}{\pi g}\exp\left[-\frac{(\mathbf{c}-\mathbf{v})\cdot(\mathbf{c}-\mathbf{v})}{gy}\right] \tag{26}$$

2.3. Proof of the positivity of entropy production in the Boltzmann model

To obtain the entropy balance equation: (i) Equation (1) (no external forces) is multiplied by $-\ln(Af)$; (ii) the result is integrated with respect to the particle velocities in the x- and z-directions, i.e., c_x and c_z; and (iii) the statement of the second law of thermodynamics is invoked. The resulting expression is as follows:

$$\frac{\partial S}{\partial t}+\nabla\cdot(\mathbf{v}S)-\nabla\cdot\int_{-\infty}^{\infty}\int_{-\infty}^{\infty}(\mathbf{c}-\mathbf{v})f\ln(Af)\,\mathrm{d}c_x\,\mathrm{d}c_z=-\int_{-\infty}^{\infty}\int_{-\infty}^{\infty}\frac{h-f}{\tau}\ln(Af)\,\mathrm{d}c_x\,\mathrm{d}c_z \tag{27}$$

In Equation (27), the first term is the local rate of change of entropy, the second term is the entropy transport due to mean advection, and third term is the entropy dispersive flux term due to particles moving at velocities different form the mean flow velocity. The right-hand side of Equation (27) is the rate of entropy production, which must be non-negative for the Boltzmann model to satisfy the second law of thermodynamics. Denote this production term as σ such that

$$\sigma=-\frac{1}{\tau}\int_{-\infty}^{\infty}\int_{-\infty}^{\infty}(h-f)\ln(Af)\,\mathrm{d}c_x\,\mathrm{d}c_z \tag{28}$$

Combination of the equilibrium distribution function (26) with the compatibility conditions (8)–(10) allows the integral of $(h-f)\ln(Ah)$ to be shown to be zero as follows:

$$\int_{-\infty}^{\infty}\int_{-\infty}^{\infty}(h-f)\ln(Ah)\,\mathrm{d}c_x\,\mathrm{d}c_z$$

$$=\int_{-\infty}^{\infty}\int_{-\infty}^{\infty}(h-f)\,\mathrm{d}c_x\,\mathrm{d}c_z-\frac{1}{gy}\int_{-\infty}^{\infty}\int_{-\infty}^{\infty}(\mathbf{c}-\mathbf{v})\cdot(\mathbf{c}-\mathbf{v})(h-f)\,\mathrm{d}c_x\,\mathrm{d}c_z=0 \tag{29}$$

Thus, addition of Equation (29) to Equation (28) produces

$$\sigma=\frac{1}{\tau}\int_{-\infty}^{\infty}\int_{-\infty}^{\infty}(h-f)\ln\frac{h}{f}\,\mathrm{d}c_x\,\mathrm{d}c_z \tag{30}$$

Now, based on Equation (30), the following conclusions about σ are obtained:

when $h<f$, then $h-f<0$ and $\ln\dfrac{h}{f}<0$ such that $\sigma>0$

when $h<f$, then $h-f>0$ and $\ln\dfrac{h}{f}>0$ such that $\sigma>0$

when $h=f$, then $h-f=0$ and $\ln\dfrac{h}{f}=0$ such that $\sigma=0$

That is

$$\sigma\geq 0 \text{ for all } f \text{ and } \sigma=0 \text{ only if } h=f \tag{31}$$

The positivity of the entropy production ensures that solutions based on the collisional Boltzmann equations are physical.

In a classic paper, Lax wrote [28]

> The role of the entropy condition is to distinguish those discontinuous solutions which are physically realizable from those which are not.

For example, the positivity of entropy production ensures that a hydraulic jump involves flow transition from supercritical to subcritical and never a transition from subcritical to supercritical conditions. Note that the equations of mass and momentum across a jump may be satisfied for either type of transition, but the only physically attainable solution is the one where entropy production is positive (i.e., $\sigma > 0$) corresponding to a transition from supercritical to subcritical. In fact, models based on conservation of mass and momentum only (e.g., Euler equations and the shallow water equations) may admit solutions that violate the entropy principle [28]. It is for this reason that physical application of these models always requires a numerical entropy fix.

Before we proceed to the formulation of the Boltzmann based numerical model for open channel flows, it is essential to ensure that the solution vector $(y, \mathbf{v})$ obtained from the Boltzmann equation is consistent with the macroscopic equations, namely the conservation laws of mass and momentum (i.e., the shallow water equation). The following section is devoted to this task.

2.4. Consistency for the Boltzmann model with mass and momentum balance

The Boltzmann based mass, x momentum, and z momentum equations are obtained by the following steps: (i) multiply Equation (1) by 1, c_x, and c_z respectively; (ii) integrate each of these three equations over c_x and c_z space; (iii) invoke definitions (3), (4), (8), and (9); and (iv) use the fact that f and $f\mathbf{c}$ have compact supports. The details of this derivation are given in Appendix C. The resulting mass and momentum equations are

$$\frac{\partial y}{\partial t} + \nabla\cdot(\mathbf{v}y) = 0 \tag{32}$$

$$\frac{\partial \mathbf{v}y}{\partial t} + \nabla\cdot\left(\mathbf{v}\mathbf{v}y + \frac{gy^2}{2}\mathbf{I}\right) + gy(\mathbf{S}_f - \mathbf{S}_0)$$

$$= \underbrace{\tau\left\{\nabla\cdot\left(\frac{gy^2}{2}\nabla\mathbf{v}\right) + \nabla\left[\mathbf{v}\cdot\nabla\left(\frac{gy^2}{2}\right)\right] - \nabla\cdot\left[\mathbf{v}\nabla\left(\frac{gy^2}{2}\right)\right]\right\}}_{\mathrm{I}} \tag{33}$$

The Boltzmann based mass conservation equation (32) is identical to its shallow water counterpart, while the Boltzmann based momentum equation (33) differs from the shallow water equation by the presence of the non-zero terms on the right-hand side. As $\tau \to 0$, the Boltzmann based momentum equation collapses to the shallow water set. Let $(y_\tau, \mathbf{v}_\tau)$ be the solution of Equations (32) and (33); and let $(y, \mathbf{v})$ be the solution of the shallow water equations. These solution sets are related according to

$$(y, \mathbf{v}) = \lim_{\tau \to 0} (y_\tau, \mathbf{v}_\tau) \tag{34}$$

A solution obtained in the limit of Equation (34) is unique and physically realizable in that it meets the entropy condition [28–30]. Therefore, a simulation algorithm developed for the Boltzmann based mass and momentum equations (32) and (33) does not require additional numerical entropy fixes.

According to Equation (34), the solution of the shallow water equations is the limit of the Boltzmann solution when $\tau \to 0$. If a numerical solution is generated using a time step Δt, the smallest resolvable time scale of the solution is of $O(\Delta t)$ [4]. Therefore, the numerical solution $(y, \mathbf{v})$ becomes

$$(y, \mathbf{v}) = \lim_{\tau \to O(\Delta t)} (y_\tau, \mathbf{v}_\tau) \tag{35}$$

An explicit form for τ in this limit is developed later in the paper.

3. NUMERICAL SOLUTION OF THE TWO-DIMENSIONAL BOLTZMANN BASED MODEL FOR OPEN CHANNEL FLOWS

Figure 1 depicts a typical spatial gird at time level n. Cell (i, j) is the dashed rectangle, whose center is node (i, j). The interface between cell (i, j) and cell $(i+1, j)$ is located at $x = x_{i+1/2}$. Similarly, the interface between cell (i, j) and cell $(i, j+1)$ is located at $z = z_{j+1/2}$.

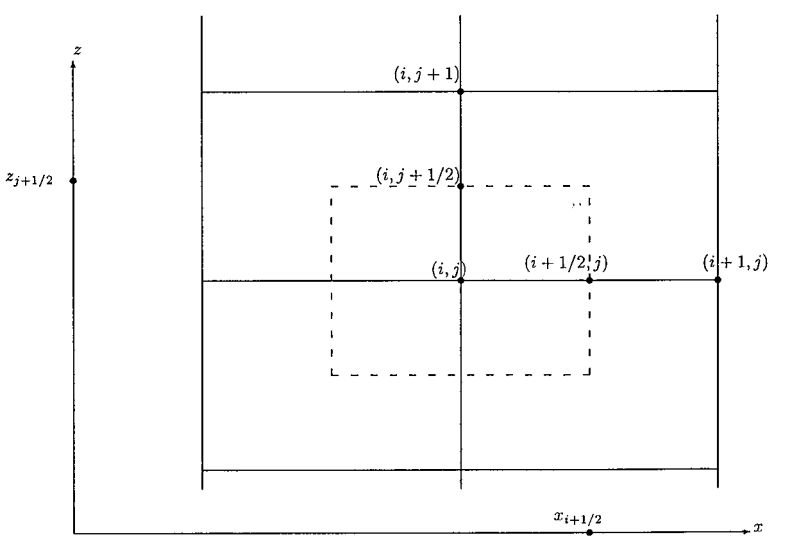

Figure 1. A typical spacial grid.

The formulation of the Boltzmann numerical scheme for shallow water equations consists of the following three main steps:

1. A data reconstruction technique, where interpolation is used to determine the functions $y^n(\mathbf{x})$ and $\mathbf{v}^n(\mathbf{x})$ from the known nodal values $y^n_{i,j}$ and $\mathbf{v}^n_{i,j}$. The functions $y^n(\mathbf{x})$ and $\mathbf{v}^n(\mathbf{x})$ are the initial conditions for the calculation of the solution at time $n+1$.
2. Formulation of a discrete Boltzmann equation.
3. Formulation of the discrete system equation for the unknown values $y^{n+1}_{i,j}$ and $\mathbf{v}^{n+1}_{i,j}$ from the discrete Boltzmann equation. It must be emphasized that the discrete Boltzmann is not coded but only used as an intermediate step in the formulation of the discrete shallow water equations. In essence, the Boltzmann equation provides an alternate formulation approach to the classical approaches based on finite elements, finite difference, Riemann solvers, and the method of characteristics.

3.1. Data reconstruction

Approximations for $y^n(\mathbf{x})$ and $(y\mathbf{v})^n(\mathbf{x})$ can be constructed form nodal values of the first derivatives of these functions using Taylor series expansions in space. These functions provide the initial conditions at time level n for marching to level $n+1$. Second-order Taylor series expansions for $y^n(\mathbf{x})$ and $(y\mathbf{v})^n(\mathbf{x})$ in cell (i,j), around node (i,j), are obtained as

$$\begin{pmatrix} y \\ \mathbf{v}y \end{pmatrix}^n = \begin{pmatrix} y \\ \mathbf{v}y \end{pmatrix}^n_{i,j} + (\mathbf{x}-\mathbf{x}_{i,j})\cdot\nabla\begin{pmatrix} y \\ \mathbf{v}y \end{pmatrix}^n_{i,j} \tag{36}$$

where $x, z \in [x_{i-1/2}, x_{i+1/2}] \times [z_{j-1/2}, z_{j+1/2}]$ and approximations to the first derivatives are employed. If first-order approximation of these derivatives are used the numerical solution is poor. Excessive smearing is obtained in the vicinity of large gradients, and the first-order character of the overall solution provides inadequate accuracy in the smooth region [30]. On the other hand, second-order approximation of the derivatives can result in unphysical oscillations near large gradients [30,31]. Two numerical approaches are commonly employed for dealing with these oscillations: artificial dissipation and slope limiters.

The primary goal of artificial dissipation is to suppress numerical oscillations that develop in the course of the generation of the solutions [31]. The drawback of artificial dissipation is best summarized by LeVeque [30, p. 175]

> The difficulty with the artificial viscosity approach is that it is hard to determine an appropriate form for [artificial viscosity] that introduces just enough dissipation to preserve the monotonicity without causing unnecessary smearing.

Even if an appropriate form of artificial viscosity is found, the magnitude of artificial dissipation coefficient has to be adjusted empirically [31].

While artificial dissipation is designed to suppress oscillations that develop in a solution, slope limiters prevent oscillations from developing [31]. In addition, slope limiters are free of empirical coefficients [30]. In this paper, the x and z derivatives in Equation (36) are determined using the monotonic upstream centered scheme for conservation laws (MUCSCL)

[32]. This limiter examines alternative approximations to the derivative terms and selects the form that will be free of oscillations. Use of this limiter to approximate the derivatives is as follows:

$$\frac{\partial}{\partial x}\begin{pmatrix} y \\ y\mathbf{v} \end{pmatrix}^n_{i,j} = \frac{1}{\Delta x}\begin{Bmatrix} \dfrac{\operatorname{sgn}(\Delta_x y^n_{i,j}) + \operatorname{sgn}(\nabla_x y^n_{i,j})}{2} \min(|\delta_x y^n_{i,j})|, |\Delta_x y^n_{i,j}|, |\nabla_x y^n_{i,j}|) \\ \dfrac{\operatorname{sgn}(\Delta_x (yu)^n_{i,j}) + \operatorname{sgn}(\nabla_x (yu)^n_{i,j})}{2} \min(|\delta_x (yu)^n_{i,j})|, |\Delta_x (yu)^n_{i,j}|, |\nabla_x (yu)^n_{i,j}|) \\ \dfrac{\operatorname{sgn}(\Delta_x (yv)^n_{i,j}) + \operatorname{sgn}(\nabla_x (yv)^n_{i,j})}{2} \min(|\delta_x (yv)^n_{i,j})|, |\Delta_x (yv)^n_{i,j}|, |\nabla_x (yv)^n_{i,j}|) \end{Bmatrix} \tag{37}$$

and

$$\frac{\partial}{\partial z}\begin{bmatrix} y \\ yu \\ yv \end{bmatrix}^n_{i,j} = \frac{1}{\Delta z}\begin{Bmatrix} \dfrac{\operatorname{sgn}(\Delta_z y^n_{i,j}) + \operatorname{sgn}(\nabla_z y^n_{i,j})}{2} \min(|\delta_z y^n_{i,j})|, |\Delta_z y^n_{i,j}|, |\nabla_z y^n_{i,j}|) \\ \dfrac{\operatorname{sgn}(\Delta_z (yu)^n_{i,j}) + \operatorname{sgn}(\nabla_z (yu)^n_{i,j})}{2} \min(|\delta_z (yu)^n_{i,j})|, |\Delta_z (yu)^n_{i,j}|, |\nabla_z (yu)^n_{i,j}|) \\ \dfrac{\operatorname{sgn}(\Delta_z (yv)^n_{i,j}) + \operatorname{sgn}(\nabla_z (yv)^n_{i,j})}{2} \min(|\delta_z (yv)^n_{i,j})|, |\Delta_z (yv)^n_{i,j}|, |\nabla_z (yv)^n_{i,j}|) \end{Bmatrix} \tag{38}$$

where the difference operators are defined as

$$\Delta_x(\,.\,)^n_{i,j} = (\,.\,)^n_{i+1,j} - (\,.\,)^n_{i,j} \tag{39}$$

$$\Delta_z(\,.\,)^n_{i,j} = (\,.\,)^n_{i,j+1} - (\,.\,)^n_{i,j} \tag{40}$$

$$\nabla_x(\,.\,)^n_{i,j} = (\,.\,)^n_{i,j} - (\,.\,)^n_{i-1,j} \tag{41}$$

$$\nabla_z(\,.\,)^n_{i,j} = (\,.\,)^n_{i,j} - (\,.\,)^n_{i,j-1} \tag{42}$$

$$\delta_x(\,.\,)^n_{i,j} = \frac{1}{2}[\Delta_x(\,.\,)^n_{i,j} + \nabla_x(\,.\,)^n_{i,j}] \tag{43}$$

$$\delta_z(\,.\,)^n_{i,j} = \frac{1}{2}[\Delta_z(\,.\,)^n_{i,j} + \nabla_z(\,.\,)^n_{i,j}] \tag{44}$$

It is worth emphasizing that limiters are designed to suppress oscillations whose origins are not in the physics of the problem under consideration but are in a numerical approximation.

These limiters do not enforce a physical requirement that an entropy condition be satisfied. For example, in studying Burger's equation for an initial square wave, Hirsch [31] found that the MacCormack scheme with the van Leer limiter prevents the occurrence of oscillations but admits entropy violating solutions. The present scheme relies on the van Leer limiter simply to prevent the occurrence of unphysical numerical oscillations in the y, yu and yv solutions. It is the collision term in the Boltzmann equation that ensures that the entropy condition is met (see Equation (31)).

At this stage, the functions $y^n(\mathbf{x})$ and $(y\mathbf{v})^n(\mathbf{x})$ in each cell (i, j) are completely specified. Thus, the first derivatives of these functions may be calculated in each cell and evaluated at the cell boundaries. These quantities are needed during the formulation of the discrete Boltzmann equation. It is very important to note that because each function is defined locally within a cell, neither its value nor its derivatives are necessarily continuous at the interfaces between cells. For examples, $(y, y\mathbf{v})^n_{i+1/2^-,j}$ is, generally, different from $(y, y\mathbf{v})^n_{i+1/2^+,j}$, where the subscript $i+1/2^+$ is used to denote that $x \to x_{i+1/2}$ with $x > x_{i+1/2}$ and the subscript $i+1/2^-$ is used to denote that $x \to x_{i+1/2}$ with $x < x_{i+1/2}$. Therefore, some procedure must be implemented to determine unique interface values, designated using overbars as, for example, $(\bar{y}, \overline{y\mathbf{v}})^n_{i+1/2,j}$ from the known quantities $(y, y\mathbf{v})^n_{i+1/2^-,j}$ and $(y, y\mathbf{v})^n_{i+1/2^+,j}$. The approach will be illustrated here for the $(i+1/2, j)$ interface with extension to other interfaces being completely analogous. In the remainder of this paper, overbars are used to denote functions that are uniquely defined at interfaces. However, the derivatives of these functions in the direction normal to an interface are not necessarily continuous.

Equations (3) and (4) are employed to obtain the function values at the interface as follows:

$$\bar{y}^n_{i+1/2,j} = \int_{-\infty}^{\infty}\int_{-\infty}^{\infty} f^n_{i+1/2,j}\,\mathrm{d}c_x\,\mathrm{d}c_z \tag{45}$$

$$(\overline{y\mathbf{v}})^n_{i+1/2,j} = \int_{-\infty}^{\infty}\int_{-\infty}^{\infty} \mathbf{c} f^n_{i+1/2,j}\,\mathrm{d}c_x\,\mathrm{d}c_z \tag{46}$$

While $f^n_{i+1/2,j}$ and $f^n_{i,j+1/2}$ can experience a jump across cell interfaces, the flow within each cell is assumed to be in local equilibrium. Therefore

$$f^n_{i+1/2} = \begin{cases} h^n_{i+1/2^-,j} & \text{if } x = x_{i+1/2^-} \\ h^n_{i+1/2^+,j} & \text{if } x = x_{i+1/2^+} \end{cases} \tag{47}$$

Insertion of Equation (47) into Equations (45) and (46) and realizing that only those particles with (a) positive x-speed (i.e., $c_x \geq 0$) will travel from $x_{i+1/2-}$ towards $x_{i+1/2}$, and (b) negative x-speed (i.e., $c_x < 0$) will travel from $x_{i+1/2+}$ towards $x_{i+1/2}$, gives

$$\bar{y}^n_{i+1/2,j} = \int_{-\infty}^{\infty}\int_{-\infty}^{0} h^n_{i+1/2^+,j}\,\mathrm{d}c_x\,\mathrm{d}c_z + \int_{-\infty}^{\infty}\int_{0}^{\infty} h^n_{i+1/2^-,j}\,\mathrm{d}c_x\,\mathrm{d}c_z \tag{48}$$

$$(\overline{y\mathbf{v}})^n_{i+1/2,j} = \int_{-\infty}^{\infty}\int_{-\infty}^{0} \mathbf{c}h^n_{i+1/2^+,j}\,\mathrm{d}c_x\,\mathrm{d}c_z + \int_{-\infty}^{\infty}\int_{-\infty}^{0} \mathbf{c}h^n_{i+1/2^-,j}\,\mathrm{d}c_x\,\mathrm{d}c_z \tag{49}$$

Evaluation of the integrals gives (see Appendix B)

$$\bar{y}^n_{i+1/2,j} = \left[\frac{y}{2}\,\mathrm{erfc}\left(\frac{u}{\sqrt{gy}}\right)\right]^n_{i+1/2^+,j} + \left[\frac{y}{2}\,\mathrm{erfc}\left(-\frac{u}{\sqrt{gy}}\right)\right]^n_{i+1/2^-,j} \tag{50}$$

$$\begin{aligned}(\overline{yu})^n_{i+1/2,j} = &\left[\frac{yu}{2}\,\mathrm{erfc}\left(\frac{u}{\sqrt{gy}}\right) - \frac{y\sqrt{gy}}{2}\,\mathrm{e}^{-u^2/gy}\right]^n_{i+1/2^+,j}\\ &+ \left[\frac{yu}{2}\,\mathrm{erfc}\left(-\frac{u}{\sqrt{gy}}\right) + \frac{y\sqrt{gy}}{2}\,\mathrm{e}^{-u^2/gy}\right]^n_{i+1/2^-,j}\end{aligned} \tag{51}$$

$$(\overline{yv})^n_{i+1/2,j} = \left[\frac{yv}{2}\,\mathrm{erfc}\left(\frac{u}{\sqrt{gy}}\right)\right]^n_{i+1/2^+,j} + \left[\frac{yv}{2}\,\mathrm{erfc}\left(-\frac{u}{\sqrt{gy}}\right)\right]^n_{i+1/2^-,j} \tag{52}$$

The analogous integrals for quantities evaluated at an $(i, j+1/2)$ interface are

$$\bar{y}^n_{i,j+1/2} = \left[\frac{y}{2}\,\mathrm{erfc}\left(\frac{v}{\sqrt{gy}}\right)\right]^n_{i,j+1/2^+} + \left[\frac{y}{2}\,\mathrm{erfc}\left(-\frac{v}{\sqrt{gy}}\right)\right]^n_{i,j+1/2^-} \tag{53}$$

$$(\overline{yu})^n_{i,j+1/2} = \left[\frac{yu}{2}\,\mathrm{erfc}\left(\frac{v}{\sqrt{gy}}\right)\right]^n_{i,j+1/2^+} + \left[\frac{yu}{2}\,\mathrm{erfc}\left(-\frac{v}{\sqrt{gy}}\right)\right]^n_{i,j+1/2^-} \tag{54}$$

$$\begin{aligned}(\overline{yv})^n_{i,j+1/2} = &\left[\frac{yv}{2}\,\mathrm{erfc}\left(\frac{v}{\sqrt{gy}}\right) - \frac{y\sqrt{gy}}{2}\,\mathrm{e}^{-v^2/gy}\right]^n_{i,j+1/2^+}\\ &+ \left[\frac{yv}{2}\,\mathrm{erfc}\left(-\frac{v}{\sqrt{gy}}\right) + \frac{y\sqrt{gy}}{2}\,\mathrm{e}^{-v^2/gy}\right]^n_{i,j+1/2^-}\end{aligned} \tag{55}$$

where erfc is the complementary error function, where $\mathrm{erfc}(\zeta) = 2/\sqrt{\pi}\int_{\zeta}^{\infty}\mathrm{e}^{-r^2}\,\mathrm{d}r$ [33, p. 297].

With this information, unique interface values for $(y, y\mathbf{v})$ have been obtained. The derivatives associated with the interface values are then defined as

$$\frac{\partial}{\partial x}\begin{pmatrix}\bar{y}\\ \overline{y\mathbf{v}}\end{pmatrix}^n_{i+1/2^-,j} = \frac{2}{\Delta x}\begin{pmatrix}\bar{y}^n_{i+1/2,j} - y^n_{i,j}\\ (\overline{y\mathbf{v}})^n_{i+1/2,j} - (yv)^n_{i,j}\end{pmatrix} \tag{56}$$

$$\frac{\partial}{\partial x}\begin{pmatrix}\bar{y}\\ \overline{y\mathbf{v}}\end{pmatrix}^n_{i+1/2^+,j} = \frac{2}{\Delta x}\begin{pmatrix}y^n_{i+1,j} - \bar{y}^n_{i+1/2,j}\\ (yv)^n_{i+1,j} - (\overline{y\mathbf{v}})^n_{i+1/2,j}\end{pmatrix} \tag{57}$$

$$\frac{\partial}{\partial z}\begin{pmatrix}\bar{y}\\ \overline{y\mathbf{v}}\end{pmatrix}^n_{i,j+1/2-}=\frac{2}{\Delta z}\begin{pmatrix}\bar{y}^n_{i,j+1/2}-y^n_{i,j}\\ (\overline{y\mathbf{v}})^n_{i,j+1/2}-(y\mathbf{v})^n_{i,j}\end{pmatrix} \tag{58}$$

$$\frac{\partial}{\partial z}\begin{pmatrix}\bar{y}\\ \overline{y\mathbf{v}}\end{pmatrix}^n_{i,j+1/2+}=\frac{2}{\Delta z}\begin{pmatrix}y^n_{i,j+1}-\bar{y}^n_{i,j+1/2}\\ (y\mathbf{v})^n_{i,j+1}-(\overline{y\mathbf{v}})^n_{i,j+1/2}\end{pmatrix} \tag{59}$$

These derivatives are required in the next section.

The unique equilibrium distribution function is designed as $\bar{h}$. The analytical expression for $\bar{h}$ at an interface can be obtained by replacing $(y, y\mathbf{v})$ in Equation (26) with $(\bar{y}, \overline{y\mathbf{v}})$. For example, $\bar{h}$ at cell interface $(i+1/2, j)$ is as follows:

$$\bar{h}^n_{i+1/2,j}=\frac{1}{\pi g}\left\{\exp\left[-\frac{(\mathbf{c}-\bar{\mathbf{v}})\cdot(\mathbf{c}-\bar{\mathbf{v}})}{g\bar{y}}\right]\right\}^n_{i+1/2,j} \tag{60}$$

In addition to $(\bar{y}, \overline{y\mathbf{v}})$ and $\bar{h}$ being uniquely specified at cell interfaces, the z and t derivatives of $\bar{h}$ are continuous (i.e., uniquely determined) at cell interfaces $(i+1/2, j)$ while the x and t derivatives of $\bar{h}$ are unique at the cell interfaces $(i, j+1/2)$. Therefore

$$\left(\bar{h}, \frac{\partial\bar{h}}{\partial z}, \frac{\partial\bar{h}}{\partial t}\right)^n_{i+1/2+,j}=\left(\bar{h}, \frac{\partial\bar{h}}{\partial z}, \frac{\partial\bar{h}}{\partial t}\right)^n_{i+1/2-,j} \tag{61}$$

$$\left(\bar{h}, \frac{\partial\bar{h}}{\partial x}, \frac{\partial\bar{h}}{\partial t}\right)^n_{i,j+1/2+}=\left(\bar{h}, \frac{\partial\bar{h}}{\partial x}, \frac{\partial\bar{h}}{\partial t}\right)^n_{i,j+1/2-} \tag{62}$$

However, the x derivatives of $\bar{h}$ at cell interfaces $x_{i+1/2}$ as given by Equations (56) and (57) may have different values; and the z derivatives of $\bar{h}$ at interfaces $z_{j+1/2}$ given by Equations (58) and (59) are also not necessarily equal. These remarks are utilized in the next section, where a discrete model for the Boltzmann equation is formulated.

3.2. Formulation of a discrete model for the Boltzmann equation

Flow discontinuities, such as hydraulic jumps, are non-equilibrium flows. However, near equilibrium, quantities such as h, y, and $\mathbf{v}$ are continuous. Since overbars are used to designate continuous functions, the equilibrium distribution h that appears in the collision term in the Boltzmann equation is replaced by $\bar{h}$. In addition, for convenience, in the remainder of this paper $\mathbf{c}$ is dropped from the explicit list of arguments of f, h, and $\bar{h}$. For example, $f(\mathbf{x}, \mathbf{c}, t)$ will be simply written as $f(\mathbf{x}, t)$. However, it is understood that f, h, and $\bar{h}$ do depend on $\mathbf{c}$.

3.2.1. Solution for f at $\boldsymbol{x}_{i+1/2,j}$. Using operator splitting [30,31,34], Equation (1) can be re-written as follows:

$$\frac{\partial f^*}{\partial t} + (\mathbf{S}_0 - \mathbf{S}_f)\cdot\frac{\partial f^*}{\partial \mathbf{c}} = 0 \quad \text{where } f^*(x, c, t = n\Delta t) = f(x, c, t) \tag{63}$$

$$\frac{\partial f^{**}}{\partial t} + \mathbf{c}\cdot\nabla f^{**} = \frac{\bar{h} - f^{**}}{\tau} \quad \text{where } f^{**}(x, c, t = n\Delta t) = f^*(x, c, t) \tag{64}$$

Note that the uniquely defined local equilibrium distribution $\bar{h}$ is used in the collision term.

If the external forces are zero (i.e., $\mathbf{S}_0 - \mathbf{S}_f = 0$), the solution operator of problem (63) is the identity operator making the solution operator of problem (64) identical to that of the solution operator of the Boltzmann equation. That is, the above operator splitting is exact in the case of zero external forces. However, if $\mathbf{S}_0 - \mathbf{S}_f$ is different from zero, the product of the solution operators of problems (63) and (64) differs from the solution operator of the full Boltzmann equation. As result, the formal accuracy of the solution based on the operator splitting is reduced. The reduction in the formal accuracy depends on the relative magnitude of the external forces and the other terms in the momentum equation. In this paper, the main objective is to test the capability of the Boltzmann scheme in modeling complex flow features, such as discontinuous solutions, extreme expansion waves, and the interactions of discontinuous and expansion waves. Near these complex flow features, $\mathbf{S}_0 - \mathbf{S}_f$ is either small or zero. In fact, as the example section shows, the splitting approximation yields accurate results for the problems considered. This implies that, for problems in open channels where flow variations are rapid, the reduction in the order of accuracy of the solution due to the splitting approximation is insignificant. However, it is expected that this conclusion may not be true for gradually varying open channel flow problems.

3.2.2. Solution for f^{**} at $\boldsymbol{x}_{i+1/2,j}$. The problem given by Equation (64) has the following characteristic equation form:

$$\frac{\mathrm{d}f^{**}}{\mathrm{d}t} = \frac{\bar{h} - f^{**}}{\tau} \quad \text{if } \frac{\mathrm{d}\mathbf{x}}{\mathrm{d}t} = \mathbf{c} \tag{65}$$

For convenience, the superscript ** will be dropped. That is, in the remainder of this paper, f^{**} is simply denoted by f. The analytical solution for f at an interface between cells located at $\mathbf{x}_{i,j}$ and $\mathbf{x}_{i+1,j}$, $f(\mathbf{x}_{i+1/2,j}, t)$, is obtained from the operator that does not explicitly involve the external forces (i.e., Equation (65)) as follows:

$$f(\mathbf{x}_{i+1/2,j}, t) = \underbrace{f(\mathbf{X}_{i+1/2,j}, t^n)}_{\mathrm{I}}\, \mathrm{e}^{-(t-t^n)/\tau} + \frac{1}{\tau}\underbrace{\int_{t^n}^{t} \bar{h}(\mathbf{x}(\beta), \beta)\, \mathrm{e}^{-(t-\beta)/\tau}\, \mathrm{d}\beta}_{\mathrm{II}} \tag{66}$$

where

$$\mathbf{X}_{i1/2,j} = \mathbf{x}_{i+1/2,j} - \mathbf{c}(t - t^n) \tag{67}$$

where β is a dummy variable. Physically, the quantity $\mathbf{X}_{i+1/2,j}$ is the co-ordinate at time t^n of a particle whose velocity is $\mathbf{c}$, which arrives at the cell interface ($\mathbf{x}_{i+1/2,j}$) at time t. Equation (67) defines particle paths during the time interval (t^n, t) for the case of no external forces. From Equation (67), the following relations hold:

$$X_{i+1/2} > x_{i+1/2} \quad \text{if } c_x < 0, \qquad X_{i+1/2} \le x_{i+1/2} \quad \text{if } c_x \ge 0 \tag{68}$$

$$Z_j > z_j \quad \text{if } c_z < 0, \qquad Z_j \le z_j \quad \text{if } c_z \ge 0 \tag{69}$$

The explicit evaluation of $f(\mathbf{x}_{i+1/2,j}, t)$ requires expressions for (a) particle locations at time t^n, namely $\mathbf{X}_{i+1/2,j}$ (already given by Equation (67)), (b) collision time τ; and (c) terms I and II in Equation (66). Expression for τ and terms I and II are developed below.

3.2.3. Collision time. Appendix C shows that the viscous terms for a Newtonian fluid are obtained by setting $\tau = \nu/gy$, where ν is the kinematic viscosity of the fluid (water in this case). However, for the numerical calculations, an expression for τ similar to that derived by Xu *et al*. [5] for the computation of shocks in compressible flows is adopted in this paper. Its form at cell interface $i+1/2$ is as follows:

$$\tau^n_{i+1/2} = C_1 \frac{\nu}{g[y]^n_{i+1/2,j}} + C_2 \frac{\left|[y^2]^n_{i+1/2+,j} - [y^2]^n_{i+1/2-,j}\right|}{[y^2]^n_{i+1/2+,j} + [y^2]^n_{i+1/2-,j}} \Delta t \quad \text{for } z \in [z_{j-1/2}, z_{j+1/2}] \tag{70}$$

where C_1 and C_2 are constants to be determined from numerical experimentation. The collision time in Equation (70) takes on a different value at each cell interface depending on the flow situation in the two adjacent cells.

Xu *et al*. [5] found that C_1 and C_2 values of order 0.01 and 1 respectively were suitable for shock calculations in gas dynamics and that their results were not very sensitive to either coefficient. The computational experiments (given later in the paper) confirm that C_2 of order 1 is also appropriate for open channel flow calculations. Note that the τ formula (i.e., Equation (70)) consists of two parts: a physical part accounted for in the first term and a numerical part accounted for by the second term. Because the viscous terms are ignored in shallow water calculations, the natural choice is to set $C_1 = 0$. However, in implementation, C_1 is set to be of order 0.001 to ensure that the collision time, as represented by τ, is never zero thereby avoiding a singularity. To explain, the Boltzmann equation has a singularity at $\tau = 0$. In flow regions where the water depth is constant, the second term in the right-hand side of Equation (70) is zero. In this instance, if C_1 was zero, the singular condition would result. The numerical part of τ ensures that model does not violate the entropy condition.

3.2.4. Approximate expression for $f(\mathbf{X}_{i+1/2,j}, t^n)$. As noted previously, flow properties (i.e., y and $y\mathbf{v}$) can experience large variations at a cell interface due, for example, to the presence of a jump or a bore. That is, generally, y and $y\mathbf{v}$ are discontinuous at cell interfaces. As a result, f usually experiences a jump across a cell interface, for example, at $x_{i+1/2}$. While $f(\mathbf{x}_{i+1/2,j}, t^n)$ may be discontinuous, the flow within each cell is considered to be in local equilibrium. Second-order Taylor series expansions for f around the co-ordinates $\mathbf{x}_{i+1/2-,j}$ and $\mathbf{x}_{i+1/2+,j}$ at t^n are developed as follows:

$$f(\mathbf{x}, t^n) = \begin{cases} h^n_{i+1/2-,j} + \nabla h^n_{i+1/2-,j} \cdot (\mathbf{x} - \mathbf{x}_{i+1/2,j}) & \text{if } x \le x_{i+1/2} \\ h^n_{i+1/2+,j} + \nabla h^n_{i+1/2+,j} \cdot (\mathbf{x} - \mathbf{x}_{i+1/2,j}) & \text{if } x > x_{i+1/2} \end{cases} \tag{71}$$

where $\mathbf{x} \in [-\infty, +\infty]$. The derivatives in Equation (71) are readily evaluated from the analytical expression for h (i.e., the Gaussian distribution). For example

$$\nabla h^n_{i+1/2-,j} = \left\{ -\nabla \left[\frac{(\mathbf{c}-\mathbf{v})\cdot(\mathbf{c}-\mathbf{v})}{gy} \right] h \right\}^n_{i+1/2-,j} \tag{72}$$

or

$$\nabla h^n_{i+1/2-,j} = \left\{ \left[-\nabla \left(\frac{\mathbf{v}\cdot\mathbf{v}}{gy} \right) + \nabla \left(\frac{2\mathbf{v}}{gy} \right) \cdot \mathbf{c} - \nabla \left(\frac{1}{gy} \right) \mathbf{c}\cdot\mathbf{c} \right] h \right\}^n_{i+1/2-,j} \tag{73}$$

Similarly

$$\nabla h^n_{i+1/2+,j} = \left\{ \left[-\nabla \left(\frac{\mathbf{v}\cdot\mathbf{v}}{gy} \right) + \nabla \left(\frac{2\mathbf{v}}{gy} \right) \cdot \mathbf{c} - \nabla \left(\frac{1}{gy} \right) \mathbf{c}\cdot\mathbf{c} \right] h \right\}^n_{i+1/2+,j} \tag{74}$$

Using vector notation, one may write the above derivatives as follows:

$$\nabla h^n_{i+1/2-,j} = \nabla \mathbf{\Phi} h^n_{i+1/2-,j} \cdot \mathbf{M} \tag{75}$$

$$\nabla h^n_{i+1/2-,j} = \nabla \mathbf{\Phi} h^n_{i+1/2-,j} \cdot \mathbf{M} \tag{76}$$

where

$$\mathbf{M} = (1, c_x, c_z, \mathbf{c}\cdot\mathbf{c})^T$$

$$\mathbf{\Phi} = \left(-\frac{\mathbf{v}\cdot\mathbf{v}}{gy}, \frac{2u}{gy}, \frac{2v}{gy}, -\frac{1}{gy} \right)$$

and the superscript T indicates the transpose. The gradient of $\mathbf{\Phi}$ has already been determined in the reconstruction stage (see Equations (37) and (38)). The approximate form for $f(\mathbf{x}, t^n)$ becomes as follows:

$$f(\mathbf{x}, t^n) = \begin{cases} h^n_{i+1/2-,j} [1 + (\mathbf{x} - \mathbf{x}_{i+1/2,j}) \cdot \nabla \mathbf{\Phi}^n_{i+1/2-,j} \cdot \mathbf{M}] & \text{if } x \le x_{i+1/2} \\ h^n_{i+1/2+,j} [1 + (\mathbf{x} - \mathbf{x}_{i+1/2,j}) \cdot \nabla \mathbf{\Phi}^n_{i+1/2+,j} \cdot \mathbf{M}] & \text{if } x > x_{i+1/2} \end{cases} \tag{77}$$

Expression (77) is valid for all $\mathbf{x}$. At $x = X_{i+1/2}$ Equation (77) becomes

$$f(\mathbf{X}_{i+1/2,j}, t^n)$$

$$= \begin{cases} h^n_{i+1/2-,j}[1 + (\mathbf{X}_{i+1/2,j} - \mathbf{x}_{i+1/2,j})\cdot\nabla\boldsymbol{\Phi}^n_{i+1/2-,j}\cdot\mathbf{M}] & \text{if } X_{i+1/2} \le x_{i+1/2} \text{ (i.e., } c_x \ge 0) \\ h^n_{i+1/2+,j}[1 + (\mathbf{X}_{i+1/2,j} - \mathbf{x}_{i+1/2,j})\cdot\nabla\boldsymbol{\Phi}^n_{i+1/2+,j}\cdot\mathbf{M}] & \text{if } X_{i+1/2} > x_{i+1/2} \text{ (i.e., } c_x < 0) \end{cases} \tag{78}$$

or

$$\begin{aligned} f(X_{i+1/2,j}, Z_j, t^n) = {} & H(c_x)h^n_{i+1/2-,j}\{1 + (\mathbf{X}_{i+1/2,j} - \mathbf{x}_{i+1/2,j})\cdot\nabla\boldsymbol{\Phi}^n_{i+1/2-,j}\cdot\mathbf{M}\} \\ & + [1 - H(c_x)]h^n_{i+1/2+,j}\{1 + (\mathbf{X}_{i+1/2,j} - \mathbf{x}_{i+1/2,j})\cdot\nabla\boldsymbol{\Phi}^n_{i+1/2+,j}\cdot\mathbf{M}\} \end{aligned} \tag{79}$$

where H is the Heaviside function (i.e., $H(c_x) = 0$ if $c_x < 0$ and $H(c_x) = 1$ if $c_x \ge 0$). Substitution of Equation (67) into this expression gives

$$\begin{aligned} f(\mathbf{X}_{i+1/2,j}, t^n) = {} & H(c_x)h^n_{i+1/2-,j}\{1 + (t - t^n)\mathbf{c}\cdot\nabla\boldsymbol{\Phi}^n_{i+1/2-,j}\cdot\mathbf{M}\} \\ & + [1 - H(c_x)]h^n_{i+1/2+,j}\{1 + (t - t^n)\mathbf{c}\cdot\nabla\boldsymbol{\Phi}^n_{i+1/2+,j}\cdot\mathbf{M}\} \end{aligned} \tag{80}$$

which completes the approximation of term I in Equation (66).

3.2.5. Approximate expression for $\bar{h}(\boldsymbol{x}, \beta)$. To evaluate the second term in Equation (66), an approximate expression for the unique equilibrium distribution $\bar{h}(\mathbf{x}, \beta)$ is required. Initially, a general approximation for $\bar{h}$ is obtained for all $\mathbf{x}$ and β. Hence, the value of $\bar{h}$ along the path defined by Equation (67) is a special case of the general formula. A second-order Taylor series expansion for $\bar{h}(\mathbf{x}, \beta)$ around the point $(\mathbf{x}_{i+1/2,j}, t^n)$ can be obtained as follows:

$$\bar{h}(\mathbf{x}, \beta) =$$

$$\begin{cases} \bar{h}^n_{i+1/2,j} + \left.\dfrac{\partial\bar{h}}{\partial x}\right|^n_{(i+1/2)-,j}(x - x_{i+1/2}) + \left.\dfrac{\partial\bar{h}}{\partial z}\right|^n_{i+1/2,j}(z - z_j) + \left.\dfrac{\partial\bar{h}}{\partial\beta}\right|^n_{i+1/2,j}(\beta - t^n) & \text{if } x \le x_{i+1/2} \text{ (i.e., } c_x \ge 0) \\ \bar{h}^n_{i+1/2,j} + \left.\dfrac{\partial\bar{h}}{\partial x}\right|^n_{(i+1/2)+,j}(x - x_{i+1/2}) + \left.\dfrac{\partial\bar{h}}{\partial z}\right|^n_{i+1/2,j}(z - z_j) + \left.\dfrac{\partial\bar{h}}{\partial\beta}\right|^n_{i+1/2,j}(\beta - t^n) & \text{if } x > x_{i+1/2} \text{ (i.e., } c_x < 0) \end{cases} \tag{81}$$

The fact that $\bar{h}$ and its z and β derivatives are unique at cell interfaces, $(i + 1/2, j)$ has been used in the formulation of Equation (81).

The derivatives of the Gaussian distribution $\bar{h}$in Equation (81) are obtained in an analogous manner to those given by Equations (73) and (74). Here the components of the gradient are written because the derivative with respect to z is continuous at the interface under consideration while the derivative with respect to x is not. The result is

$$\left[\frac{\partial \bar{h}}{\partial x}\right]^n_{i+1/2^-,j} = \left\{\left[-\frac{\partial\left(\frac{\bar{\mathbf{v}}\cdot\bar{\mathbf{v}}}{g\bar{y}}\right)}{\partial x}+\frac{\partial\left(\frac{2\bar{\mathbf{v}}}{g\bar{y}}\right)}{\partial x}\cdot\mathbf{c}-\frac{\partial\left(\frac{1}{g\bar{y}}\right)}{\partial x}\,\mathbf{c}\cdot\mathbf{c}\right]\bar{h}\right\}^n_{i+1/2^-,j} \tag{82}$$

$$\left[\frac{\partial \bar{h}}{\partial x}\right]^n_{i+1/2^+,j} = \left\{\left[-\frac{\partial\left(\frac{\bar{\mathbf{v}}\cdot\bar{\mathbf{v}}}{g\bar{y}}\right)}{\partial x}+\frac{\partial\left(\frac{2\bar{\mathbf{v}}}{g\bar{y}}\right)}{\partial x}\cdot\mathbf{c}-\frac{\partial\left(\frac{1}{g\bar{y}}\right)}{\partial x}\,\mathbf{c}\cdot\mathbf{c}\right]\bar{h}\right\}^n_{i+1/2^+,j} \tag{83}$$

$$\left[\frac{\partial \bar{h}}{\partial z}\right]^n_{i+1/2,j} = \left\{\left[-\frac{\partial\left(\frac{\bar{\mathbf{v}}\cdot\bar{\mathbf{v}}}{g\bar{y}}\right)}{\partial z}+\frac{\partial\left(\frac{2\bar{\mathbf{v}}}{g\bar{y}}\right)}{\partial z}\cdot\mathbf{c}-\frac{\partial\left(\frac{1}{g\bar{y}}\right)}{\partial z}\,\mathbf{c}\cdot\mathbf{c}\right]\bar{h}\right\}^n_{i+1/2,j} \tag{84}$$

$$\left[\frac{\partial \bar{h}}{\partial \beta}\right]^n_{i+1/2,j} = \left\{\left[-\frac{\partial\left(\frac{\bar{\mathbf{v}}\cdot\bar{\mathbf{v}}}{g\bar{y}}\right)}{\partial \beta}+\frac{\partial\left(\frac{2\bar{\mathbf{v}}}{g\bar{y}}\right)}{\partial \beta}\cdot\mathbf{c}-\frac{\partial\left(\frac{1}{g\bar{y}}\right)}{\partial \beta}\,\mathbf{c}\cdot\mathbf{c}\right]\bar{h}\right\}^n_{i+1/2,j} \tag{85}$$

Because $\bar{h}$ is continuous, $\bar{h}^n_{i+1/2^+,j} = \bar{h}^n_{i+1/2^-,j} = \bar{h}^n_{i+1/2,j}$. Using this fact and the notation introduced previously, one can write the preceding derivatives as

$$\left[\frac{\partial \bar{h}}{\partial x}\right]^n_{i+1/2^-,j} = \bar{h}^n_{i+1/2,j}\left[\frac{\partial \bar{\mathbf{\Phi}}}{\partial x}\right]^n_{i+1/2^-,j}\cdot\mathbf{M} \tag{86}$$

$$\left[\frac{\partial \bar{h}}{\partial x}\right]^n_{i+1/2^+,j} = \bar{h}^n_{i+1/2,j}\left[\frac{\partial \bar{\mathbf{\Phi}}}{\partial x}\right]^n_{i+1/2^+,j}\cdot\mathbf{M} \tag{87}$$

$$\left[\frac{\partial \bar{h}}{\partial z}\right]^n_{i+1/2,j} = \bar{h}^n_{i+1/2,j}\left[\frac{\partial \bar{\mathbf{\Phi}}}{\partial z}\right]^n_{i+1/2,j}\cdot\mathbf{M} \tag{88}$$

$$\left[\frac{\partial \bar{h}}{\partial \beta}\right]^n_{i+1/2,j} = \bar{h}^n_{i+1/2,j}\left[\frac{\partial \bar{\mathbf{\Phi}}}{\partial \beta}\right]^n_{i+1/2,j}\cdot\mathbf{M} \tag{89}$$

where

$$\bar{\Phi} = \left(-\frac{\bar{\mathbf{v}}\cdot\bar{\mathbf{v}}}{g\bar{y}}, \frac{2\bar{u}}{g\bar{y}}, \frac{2\bar{v}}{g\bar{y}}, -\frac{1}{g\bar{y}}\right)$$

Insertion of Equation (86)–(89) into Equation (81) yields the following approximate solution expression for $\bar{h}(\mathbf{x}, \beta)$:

$$\begin{aligned}\bar{h}(\mathbf{x},\beta) = \bar{h}^n_{i+1/2,j}\Bigg\{1 &+ \left(\frac{\partial \bar{\mathbf{\Phi}}}{\partial \beta}\right)^n_{i+1/2,j}\cdot\mathbf{M}(\beta - t^n) + \left(\frac{\partial \mathbf{\Phi}}{\partial z}\right)^n_{i+1/2,j}\cdot\mathbf{M}(z - z_j)\\ &+ \left[H(c_x)\left(\frac{\partial \bar{\mathbf{\Phi}}}{\partial x}\right)^n_{i+1/2^-,j} + [1 + H(c_x)]\left(\frac{\partial \bar{\mathbf{\Phi}}}{\partial x}\right)^n_{i+1/2^+,j}\right]\cdot\mathbf{M}(x - x_{i+1/2})\Bigg\}\end{aligned} \tag{90}$$

The derivatives of $\bar{\mathbf{\Phi}}$ with respect to x have already been determined in the reconstruction stage (see Equations (56) and (57)). However, the derivatives of $\bar{\mathbf{\Phi}}$ with respect to z and β at node $(i+1/2, j, n)$ are unknown. First, we evaluate the derivative $\partial\bar{\mathbf{\Phi}}/\partial z$.

The compatibility equations (8)–(10) at $\beta = t^n$ can be re-written as follows:

$$\int_{-\infty}^{\infty}\int_{-\infty}^{\infty}\frac{\bar{h}(\mathbf{x}, t^n) - f(\mathbf{x}, t^n)}{\tau^n}\mathbf{M}\,\mathrm{d}c_x\,\mathrm{d}c_z = \mathbf{0} \quad \forall\mathbf{x} \tag{91}$$

Since Equation (91) is true for all z, the following holds:

$$\frac{\partial}{\partial z}\int_{-\infty}^{\infty}\int_{-\infty}^{\infty}\frac{\bar{h}(\mathbf{x}, t^n) - f(\mathbf{x}, t^n)}{\tau^n}\mathbf{M}\,\mathrm{d}c_x\,\mathrm{d}c_z = \mathbf{0} \quad \forall\mathbf{x} \tag{92}$$

This equation may be written in a form particularly appropriate for $x = x_{i+1/2}$ as

$$\begin{aligned}&\frac{\partial}{\partial z}\int_{-\infty}^{\infty}\int_{0}^{\infty}\frac{\bar{h}(x_{i+1/2}, z, t^n) - f(x_{i+1/2-}, z, t^n)}{\tau^n_{i+1/2}}\mathbf{M}\,\mathrm{d}c_x\,\mathrm{d}c_z\\ &+\frac{\partial}{\partial z}\int_{-\infty}^{\infty}\int_{-\infty}^{0}\frac{\bar{h}(x_{i+1/2}, z, t^n) - f(x_{i+1/2+}, z, t^n)}{\tau^n_{i+1/2}}\mathbf{M}\,\mathrm{d}c_x\,\mathrm{d}c_z = \mathbf{0} \quad \forall z\end{aligned} \tag{93}$$

The quantities appearing in the integrand may be obtained from Equations (77) and (90) at t^n and $x_{i+1/2}$

$$\bar{h}(x_{i+1/2}, z, t^n) = \bar{h}^n_{i+1/2,j}\left[1 + (z - z_j)\left(\frac{\partial\bar{\mathbf{\Phi}}}{\partial z}\right)^n_{i+1/2,j}\cdot\mathbf{M}\right] \tag{94}$$

$$\begin{aligned}f(x_{i+1/2}, z, t^n) = {}& h^n_{i+1/2-,j}\left[1 + (z - z_j)\left(\frac{\partial\mathbf{\Phi}}{\partial z}\right)^n_{i+1/2-,j}\cdot\mathbf{M}\right]H(c_x)\\ &+ h^n_{i+1/2+,j}\left[1 + (z - z_j)\left(\frac{\partial\mathbf{\Phi}}{\partial z}\right)^n_{i+1/2+,j}\cdot\mathbf{M}\right][1 - H(c_x)]\end{aligned} \tag{95}$$

Substitution of these last two equations into Equation (93) while noting that $\tau^n_{i+1/2}$ is piecewise constant in z (see Equation (70)) gives

$$\begin{aligned}&\left(\frac{\partial\bar{\mathbf{\Phi}}}{\partial z}\right)^n_{i+1/2,j}\cdot\int_{-\infty}^{\infty}\int_{-\infty}^{\infty}\bar{h}^n_{i+1/2,j}\mathbf{M}\mathbf{M}\,\mathrm{d}c_x\,\mathrm{d}c_z\\ &=\left(\frac{\partial\mathbf{\Phi}}{\partial z}\right)^n_{i+1/2-,j}\cdot\int_{-\infty}^{\infty}\int_{0}^{\infty}h^n_{i+1/2-,j}\mathbf{M}\mathbf{M}\,\mathrm{d}c_x\,\mathrm{d}c_z\\ &\quad+\left(\frac{\partial\mathbf{\Phi}}{\partial z}\right)^n_{i+1/2+,j}\cdot\int_{-\infty}^{\infty}\int_{-\infty}^{0}h^n_{i+1/2+,j}\mathbf{M}\mathbf{M}\,\mathrm{d}c_x\,\mathrm{d}c_z\end{aligned} \tag{96}$$

The integrals appearing in this equation are evaluated in Appendix B as the matrices $[\bar{\Gamma}]^n_{i+1/2j}$, $[\Gamma^+_{c_x}]^n_{i+1/2-,j}$, and $[\Gamma^-_{c_x}]^n_{i+1/2+,j}$ so that the equation becomes

$$\left[\frac{\partial\bar{\mathbf{\Phi}}}{\partial z}\cdot\bar{\Gamma}\right]^n_{i+1/2,j}=\left[\frac{\partial\mathbf{\Phi}}{\partial z}\cdot\Gamma^+_{c_x}\right]^n_{i+1/2-,j}+\left[\frac{\partial\mathbf{\Phi}}{\partial z}\cdot\Gamma^-_{c_x}\right]^n_{i+1/2+,j} \tag{97}$$

where the derivatives

$$\left[\frac{\partial\mathbf{\Phi}}{\partial z}\right]^n_{i+1/2-,j}\quad\text{and}\quad\left[\frac{\partial\mathbf{\Phi}}{\partial z}\right]^n_{i+1/2+,j}$$

have previously been obtained in the data reconstruction stage. Therefore, Equation (97) may be used to determine the value of the vector of derivatives $\partial\bar{\mathbf{\Phi}}/\partial z$. Hence, $\partial\bar{\mathbf{\Phi}}/\partial\beta$ is the only remaining unknown derivative. It may be obtained after first completing the solution of the discretized Equation (66). The approximate solution for h given as $\bar{h}$ in Equation (90) is valid for all $\mathbf{x}$ and t. Invoking Equation (67) one can write expression (90) along a particle path as follows:

$$\begin{aligned}&\bar{h}(\mathbf{x}(\beta),\beta)=\\&\bar{h}^n_{i+1/2,j}\left\{1+\left(\frac{\partial\bar{\mathbf{\Phi}}}{\partial\beta}\right)^n_{i+1/2,j}\cdot\mathbf{M}(\beta-t^n)+\left(\frac{\partial\bar{\mathbf{\Phi}}}{\partial z}\right)^n_{i+1/2,j}\cdot\mathbf{M}c_z(\beta-t)\right.\\&\left.+\left[H(c_x)\left(\frac{\partial\bar{\mathbf{\Phi}}}{\partial x}\right)^n_{i+1/2-,j}+[1-H(c_x)]\left(\frac{\partial\bar{\mathbf{\Phi}}}{\partial x}\right)^n_{i+1/2+,j}\right]\cdot\mathbf{M}c_x(\beta-t)\right\}\end{aligned} \tag{98}$$

At this stage, term II in Equation (66) can be integrated with respect to β as follows:

$$\begin{aligned}&\frac{1}{\tau}\int_{t^n}^{t}\bar{h}(\mathbf{x}(\beta),\beta)\,\mathrm{e}^{-(t-\beta)/\tau}\,\mathrm{d}\beta=\bar{h}^n_{i+1/2,j}\left[\frac{1}{\tau}\int_{t^n}^{t}\mathrm{e}^{-(t-\beta)/\tau}\,\mathrm{d}\beta\right]\\&+\bar{h}^n_{i+1/2,j}\left[\frac{\partial\bar{\Phi}}{\partial\beta}\right]^n_{i+1/2,j}\cdot\mathbf{M}\left[\frac{1}{\tau}\int_{t^n}^{t}(\beta-t^n)\,\mathrm{e}^{-(t-\beta)/\tau}\,\mathrm{d}\beta\right]\\&-\bar{h}^n_{i+1/2,j}c_z\left[\frac{\partial\bar{\Phi}}{\partial z}\right]^n_{i+1/2,j}\cdot\mathbf{M}\left[\frac{1}{\tau}\int_{t^n}^{t}(t-\beta)\,\mathrm{e}^{-(t-\beta)/\tau}\,\mathrm{d}\beta\right]\\&-\bar{h}^n_{i+1/2,j}\left\{c_xH(c_x)\left[\frac{\partial\bar{\Phi}}{\partial x}\right]^n_{i+1/2-,j}+c_x[1-H(c_x)]\left[\frac{\partial\bar{\Phi}}{\partial x}\right]^n_{i+1/2+,j}\right\}\\&\cdot\mathbf{M}\left[\frac{1}{\tau}\int_{t^n}^{t}(t-\beta)\,\mathrm{e}^{-(t-\beta)/\tau}\,\mathrm{d}\beta\right]\end{aligned} \tag{99}$$

which gives the following expression:

$$\frac{1}{\tau}\int_{t^n}^{t}\bar{h}(\mathbf{x}(\beta),\beta)\,\mathrm{e}^{-(t-\beta)/\tau}\,\mathrm{d}\beta=\bar{h}^n_{i+1/2,j}\left\{1-\exp\left[-\frac{t-t^n}{\tau}\right]\right\}$$

$$+\bar{h}^n_{i+1/2,j}\left[\frac{\partial\bar{\mathbf{\Phi}}}{\partial\beta}\right]^n_{i+1/2,j}\cdot\mathbf{M}\left\{t-t^n-\tau\left[1-\exp\left(-\frac{t-t^n}{\tau}\right)\right]\right\}$$

$$-\bar{h}^n_{i+1/2,j}\left\{c_z\left[\frac{\partial\bar{\mathbf{\Phi}}}{\partial z}\right]^n_{i+1/2,j}+c_xH(c_x)\left[\frac{\partial\bar{\mathbf{\Phi}}}{\partial x}\right]^n_{i+1/2^-,j}+c_x[1-H(c_x)]\left[\frac{\partial\bar{\mathbf{\Phi}}}{\partial x}\right]^n_{i+1/2^+,j}\right\}$$

$$\cdot\mathbf{M}\left\{(t-t^n)\exp\left[-\frac{t-t^n}{\tau}\right]+\tau\left[-1+\exp\left(-\frac{t-t^n}{\tau}\right)\right]\right\} \tag{100}$$

This completes the approximation of term II in Equation (66). Insertion of Equations (80) and (100) into Equation (66) yields the following:

$$f(x_{i+1/2},z_j,t)-\bar{h}^n_{i+1/2,j}-\bar{h}^n_{i+1/2,j}\left[\frac{\partial\bar{\mathbf{\Phi}}}{\partial\beta}\right]^n_{i+1/2,j}\cdot\mathbf{M}(t-t^n)$$

$$=\mathrm{e}^{-(t-t^n)/\tau}\left\{H(c_x)h^n_{i+1/2^-,j}+[1-H(c_x)]h^n_{i+1/2^+,j}-\bar{h}^n_{i+1/2,j}\right.$$

$$-(t-t^n)\left\{H(c_x)\left[h\left(c_x\frac{\partial\mathbf{\Phi}}{\partial x}+c_z\frac{\partial\mathbf{\Phi}}{\partial z}\right)\right]^n_{i+1/2^-,j}\right.$$

$$\left.\left.+[1-H(c_x)]\left[h\left(c_x\frac{\partial\mathbf{\Phi}}{\partial x}+c_z\frac{\partial\mathbf{\Phi}}{\partial z}\right)\right]^n_{i+1/2^+,j}\right\}\cdot\mathbf{M}\right\}$$

$$-\bar{h}^n_{i+1/2,j}\left[\frac{\partial\bar{\mathbf{\Phi}}}{\partial\beta}\right]^n_{i+1/2,j}\cdot\mathbf{M}\left\{\tau\left[1-\exp\left(-\frac{t-t^n}{\tau}\right)\right]\right\}$$

$$+\bar{h}^n_{i+1/2,j}\left\{c_z\left[\frac{\partial\bar{\mathbf{\Phi}}}{\partial z}\right]^n_{i+1/2,j}+c_xH(c_x)\left[\frac{\partial\bar{\mathbf{\Phi}}}{\partial x}\right]^n_{i+1/2^-,j}+c_x[1-H(c_x)]\left[\frac{\partial\bar{\mathbf{\Phi}}}{\partial x}\right]^n_{i+1/2^+,j}\right\}$$

$$\cdot\mathbf{M}\left\{(t-t^n)\exp\left(-\frac{t-t^n}{\tau}\right)+\tau\left[-1+\exp\left(-\frac{t-t^n}{\tau}\right)\right]\right\} \tag{101}$$

This is the discrete Boltzmann equation. At this stage, the only remaining unknown is the time derivatives $\partial\bar{\mathbf{\Phi}}/\partial\beta$ at $(i+1/2,j,n)$. This time derivative is evaluated below.

Using the results in Appendix B, the zero moment of the difference equation (101) gives

$$\int_{-\infty}^{\infty}\int_{-\infty}^{\infty}\frac{f(x_{i+1/2},z_j,t)-h(x_{i+1/2},z_j,t)}{\tau}\,\mathrm{d}c_x\,\mathrm{d}c_z+\left[\frac{\partial\bar{y}}{\partial t}\right]^n_{i+1/2,j}(1-\mathrm{e}^{\eta})$$

$$
\begin{aligned}
&= -\left\{\left[\frac{\partial\left(\dfrac{yu}{2}\operatorname{erfc}\left(-\dfrac{u}{\sqrt{gy}}\right)+\dfrac{y\sqrt{gy}}{2}\,\mathrm{e}^{-y^2/gy}\right)}{\partial x}\right]_{i+1/2^-,j}^{n}\right.\\
&\quad\left.+\left[\frac{\partial\left(\dfrac{yu}{2}\operatorname{erfc}\left(\dfrac{u}{\sqrt{gy}}\right)-\dfrac{y\sqrt{gy}}{2}\,\mathrm{e}^{-y^2/gy}\right)}{\partial x}\right]_{i+1/2^+,j}^{n}\right\}\eta\ \mathrm{e}^{\eta}\\
&\quad+\left\{\left[\frac{\partial\left(\dfrac{\overline{yu}}{2}\operatorname{erfc}\left(\dfrac{-\bar{u}}{\sqrt{g\bar{y}}}\right)+\dfrac{\bar{y}\sqrt{g\bar{y}}}{2}\,\mathrm{e}^{-\bar{y}^2/g\bar{y}}\right)}{\partial x}\right]_{i+1/2^-,j}^{n}\right.\\
&\quad\left.+\left[\frac{\partial\left(\dfrac{\overline{yu}}{2}\operatorname{erfc}\left(\dfrac{\bar{u}}{\sqrt{g\bar{y}}}\right)+\dfrac{\bar{y}\sqrt{g\bar{y}}}{2}\,\mathrm{e}^{-\bar{y}^2/g\bar{y}}\right)}{\partial x}\right]_{i+1/2^+,j}^{n}\right\}\eta\ \mathrm{e}^{\eta}\\
&\quad+\left\{\left[\frac{\partial\left(\dfrac{\overline{yu}}{2}\operatorname{erfc}\left(-\dfrac{\bar{u}}{\sqrt{g\bar{y}}}\right)+\dfrac{\bar{y}\sqrt{g\bar{y}}}{2}\,\mathrm{e}^{-\bar{y}^2/g\bar{y}}\right)}{\partial x}\right]_{i+1/2^-,j}^{n}\right.\\
&\quad\left.+\left[\frac{\partial\left(\dfrac{\overline{yu}}{2}\operatorname{erfc}\left(\dfrac{\bar{u}}{\sqrt{g\bar{y}}}\right)+\dfrac{\bar{y}\sqrt{g\bar{y}}}{2}\,\mathrm{e}^{-\bar{y}^2/g\bar{y}}\right)}{\partial x}\right]_{i+1/2^+,j}^{n}\right\}(1-\mathrm{e}^{\eta})-\left[\frac{\partial\overline{yv}}{\partial x}\right]_{i+1/2,j}^{n}(1-\mathrm{e}^{\eta})
\end{aligned}
\tag{102}
$$

where $\eta=(t-t^n)/\tau$. The first bracketed term on the right-hand side defines $[\partial uy/\partial x]_{i+1/2,j}^{n}$ and the second bracketed term on the right-hand side defines $[\partial\overline{uy}/\partial z]_{i+1/2,j}^{n}$. Therefore, the above equation can be re-written as follows:

$$
\begin{aligned}
&\int_{-\infty}^{\infty}\int_{-\infty}^{\infty}\frac{f(x_{i+1/2},z_j,t)-h(x_{i+1/2},z_j,t)}{\tau}\,\mathrm{d}c_x\,\mathrm{d}c_z=\left\{\left[\frac{\partial\overline{yu}}{\partial x}\right]_{i+1/2,j}^{n}-\left[\frac{\partial yu}{\partial x}\right]_{i+1/2,j}^{n}\right\}\kappa\ \mathrm{e}^{\eta}\\
&\times\left\{\left[\frac{\partial\bar{y}}{\partial t}\right]_{i+1/2,j}^{n}+\left[\frac{\partial\overline{yu}}{\partial x}\right]_{i+1/2,j}^{n}+\left[\frac{\partial\overline{yv}}{\partial z}\right]_{i+1/2,j}^{n}\right\}(1-\mathrm{e}^{\eta})
\end{aligned}
\tag{103}
$$

Similarly, the first moment of the difference equation (101) with respect to c_x gives

$$
\begin{aligned}
&\int_{-\infty}^{\infty}\int_{-\infty}^{\infty}c_x\frac{f(x_{i+1/2},z_j,t)-h(x_{i+1/2},z_j,t)}{\tau}\,\mathrm{d}c_x\,\mathrm{d}c_z\\
&=\left\{\left[\frac{\partial\overline{yu}^2+\dfrac{g\bar{y}^2}{2}}{\partial x}\right]_{i+1/2,j}^{n}-\left[\frac{\partial yu^2+\dfrac{gy^2}{2}}{\partial x}\right]_{i+1/2,j}^{n}\right\}\eta\ \mathrm{e}^{\eta}\\
&\quad\times\left\{\left[\frac{\partial\overline{yu}}{\partial t}\right]_{i+1/2,j}^{n}+\left[\frac{\partial\overline{yu}^2+\dfrac{g\bar{y}^2}{2}}{\partial x}\right]_{i+1/2,j}^{n}+\left[\frac{\partial\overline{yuv}}{\partial z}\right]_{i+1/2,j}^{n}\right\}(1-\mathrm{e}^{\eta})
\end{aligned}
\tag{104}
$$

With the exception of the time derivative terms, all the other bracketed terms on the right-hand side of Equations (103) and (104) have already been determined. In this paper, the evaluation of the constant but unknown time derivatives on the right-hand side of Equations (103) and (104) is based on the compatibility conditions so as to ensure that the scheme conserves both mass and momentum.

In reality, the compatibility equations requires that the left-hand side of Equations (103) and (104) be zero at every instant. This would be the case if each of the bracketed terms on the right-hand side of Equations (103) and (104) were zero. Setting the second bracketed terms on the right-hand side of Equations (103) and (104) to zero solves for the unknown times derivatives. However, the first bracketed terms on the right-hand side of Equations (103) and (104) are zero only if y and u are at least C^1 continuous in the direction normal to the cell boundary. Therefore, in general it is not possible to ensure that the compatibility conditions are satisfied at every instant. However, it is possible to satisfy the compatibility conditions (i.e., mass and momentum conservation) in an average sense over a time step. This is accomplished as follows:

$$\int_{t^n}^{t^n+\Delta t}\int_{-\infty}^{\infty}\int_{-\infty}^{\infty}\frac{\bar{h}(x_{i+1/2},z_j,t)-f(x_{i+1/2},z_j,t)}{\tau_{i+1/2,j}}\mathbf{M}\,\mathrm{d}c_x\mathrm{d}c_z\,\mathrm{d}t=\mathbf{0} \tag{105}$$

Insertion of (101) into expression (105) with the restriction that in the time interval $t\in[t^n, t^n+\Delta t]$ the collision time τ is constant followed by integration of the resulting expression gives

$$\begin{aligned}
\left[\frac{\partial\bar{\mathbf{\Phi}}}{\partial t}\cdot\bar{\Gamma}\right]^n_{i+1/2,j} &= a[\bar{\mathbf{\Phi}}^n_{i+1/2,j}-\mathbf{\Phi}^n_{i+1/2^-,j}-\mathbf{\Phi}^n_{i+1/2^+,j}]\\
&+b\left[\left(\frac{\partial\bar{\mathbf{\Phi}}}{\partial x}\right)^n_{i+1/2^-,j}\cdot(\bar{\Omega}^+_{c_x})^n_{i+1/2,j}+\left(\frac{\partial\bar{\mathbf{\Phi}}}{\partial x}\right)^n_{i+1/2^+,j}\cdot(\bar{\Omega}^-_{c_x})^n_{i+1/2,j}+\left(\frac{\partial\bar{\mathbf{\Phi}}}{\partial z}\right)^n_{i+1/2,j}\cdot(\bar{\Omega})^n_{i+1/2,j}\right]\\
&+d\left[\left(\frac{\partial\mathbf{\Phi}}{\partial x}\right)^n_{i+1/2^-,j}\cdot(\bar{\Omega}^+_{c_x})^n_{i+1/2^-,j}+\left(\frac{\partial\mathbf{\Phi}}{\partial x}\right)^n_{i+1/2^+,j}\cdot(\bar{\Omega}^-_{c_x})^n_{i+1/2^+,j}\right]\\
&+d\left[\left(\frac{\partial\mathbf{\Phi}}{\partial z}\right)^n_{i+1/2^-,j}\cdot(\Upsilon^+_{c_x})^n_{i+1/2^-,j}+\left(\frac{\partial\mathbf{\Phi}}{\partial x}\right)^n_{i+1/2^+,j}\cdot(\Upsilon^-_{c_x})^n_{i+1/2^+,j}\right]
\end{aligned} \tag{106}$$

where $\alpha=-(1-\mathrm{e}^{-\Delta t/\tau})/\kappa$, $b=(-\Delta t+2\tau(1-\mathrm{e}^{-\Delta t/\tau})-\Delta t\,\mathrm{e}^{-\Delta t/\tau})/\kappa$ and $b=(-\tau(1-\mathrm{e}^{-\Delta t/\tau})+\Delta t\,\mathrm{e}^{-\Delta t/\tau})/\kappa$ and $k=\Delta t-\tau(1-\mathrm{e}^{-\Delta t/\tau})$. The matrices in Equation (106) are given in Appendix B.

3.3. Formulation of the Boltzmann based shallow water model

Equation (101) gives the discrete model of the Boltzmann equation. The aim of this section is to formulate the numerical model for shallow water equation using this discrete Boltzmann equation.

Integrating Equations (63) and (64) in a numerical cell (i,j) from the interface $x_{i-1/2}$ to $x_{i+1/2}$, $z_{j-1/2}$ to $z_{j+1/2}$ and time from t^n to t^{n+1} and combining gives

$$\int_{x_{i-1/2}}^{x_{i+1/2}}\int_{z_{j-1/2}}^{z_{j+1/2}}(f^{n+1}-f^n)\,\mathrm{d}z\,\mathrm{d}x=\int_{t^n}^{t^{n+1}}\int_{z_{j-1/2}}^{z_{j+1/2}}(f_{i-1/2}-f_{i+1/2})\,\mathrm{d}z\,\mathrm{d}t$$
$$+\int_{t^n}^{t^{n+1}}\int_{x_{i-1/2}}^{x_{i+1/2}}(f_{j-1/2}-f_{j+1/2})\,\mathrm{d}x\,\mathrm{d}t+\int_{x_{i-1/2}}^{x_{i+1/2}}\int_{z_{j-1/2}}^{z_{j+1/2}}\int_{t^n}^{t^{n+1}}(S_{0x}-S_{\mathrm{f}x})\frac{\partial f^*}{\partial c}\,\mathrm{d}t\,\mathrm{d}z\,\mathrm{d}x \tag{107}$$

Taking the zero moment, first moment in c_x, and first moment in c_y of Equation (107) and writing the result in vector form gives the following difference equations for two-dimensional shallow water problems:

$$\mathbf{W}_{i,j}^{n+1}-\mathbf{W}_{i,j}^{n}=\frac{1}{\Delta z\,\Delta x}\int_{t^n}^{t^{n+1}}\int_{z_{j-1/2}}^{z_{j+1/2}}(\mathbf{F}_{i-1/2}-\mathbf{F}_{i+1/2})\,\mathrm{d}z\,\mathrm{d}t$$
$$+\frac{1}{\Delta z\,\Delta x}\int_{t^n}^{t^{n+1}}\int_{x_{i-1/2}}^{x_{i+1/2}}(\mathbf{G}_{j-1/2}-\mathbf{G}_{j+1/2})\,\mathrm{d}x\,\mathrm{d}t+\frac{1}{\Delta z\,\Delta x}\int_{x_{i-1/2}}^{x_{i+1/2}}\int_{z_{j-1/2}}^{z_{j+1/2}}\int_{t^n}^{t^{n+1}}\mathbf{S}\,\mathrm{d}t\,\mathrm{d}z\,\mathrm{d}x \tag{108}$$

where

$$\mathbf{W}=\begin{pmatrix}y\\uy\\vy\end{pmatrix}=\begin{pmatrix}\int_{-\infty}^{\infty}\int_{-\infty}^{\infty}f\,\mathrm{d}c_x\,\mathrm{d}c_z\\ \int_{-\infty}^{\infty}\int_{-\infty}^{\infty}c_xf\,\mathrm{d}c_x\,\mathrm{d}c_z\\ \int_{-\infty}^{\infty}\int_{-\infty}^{\infty}c_zf\,\mathrm{d}c_x\,\mathrm{d}c_z\end{pmatrix},\qquad \mathbf{F}=\begin{pmatrix}\int_{-\infty}^{\infty}\int_{-\infty}^{\infty}c_xf\,\mathrm{d}c_x\,\mathrm{d}c_x\\ \int_{-\infty}^{\infty}\int_{-\infty}^{\infty}c_x^2f\,\mathrm{d}c_x\,\mathrm{d}c_z\\ \int_{-\infty}^{\infty}\int_{-\infty}^{\infty}c_xc_zf\,\mathrm{d}c_z\,\mathrm{d}c_x\end{pmatrix}$$

$$\mathbf{G}=\begin{pmatrix}\int_{-\infty}^{\infty}\int_{-\infty}^{\infty}c_zf\,\mathrm{d}c_x\,\mathrm{d}c_z\\ \int_{-\infty}^{\infty}\int_{-\infty}^{\infty}c_xc_zf\,\mathrm{d}c_z\,\mathrm{d}c_x\\ \int_{-\infty}^{\infty}\int_{-\infty}^{\infty}c_x^2f\,\mathrm{d}c_x\,\mathrm{d}c_z\end{pmatrix},\qquad \mathbf{S}=\begin{pmatrix}0\\gy(S_{0x}-S_{\mathrm{f}x})\\gy(S_{0z}-S_{\mathrm{f}x})\end{pmatrix}$$

In addition, $\Delta x=x_{i+1/2}-x_{i-1/2}$, $\Delta z=z_{j+1/2}-z_{j-1/2}$, $\Delta t=t^{n+1}-t^n$ and $\mathbf{W}_{i,j}^n$ is the average value of $\mathbf{W}$ in the cell (i,j) at time n. Physically, $\mathbf{F}$ represents the mass and momentum fluxes along x, $\mathbf{G}$ represents the mass and momentum fluxes along x, and $\mathbf{S}$ represents the net external forces along x and z.

The vector $\mathbf{W}_{i,j}^n$ in Equation (108) is known from the data reconstruction. In addition, the first and second integrals on the right-hand side of Equation (108) are obtainable from the discrete Boltzmann equation (i.e., Equation (101)). That is, the sole reason for deriving the discrete Boltzmann equation (101) is to evaluate the flux terms (i.e., the first and second integral terms) on the right-hand side of Equation (108). For example, the mass and momentum flux at $i+1/2$ is obtained from the difference from of the Boltzmann equation as follows:

$$\int_{t^n}^{t^{n+1}} \int_{z_{j-1/2}}^{z_{j+1/2}} \mathbf{F}_{i+1/2}\,\mathrm{d}z\,\mathrm{d}t = \Delta z \int_{-\infty}^{\infty} \int_{-\infty}^{\infty} \int_{t^n}^{t^{n+1}} f_{i+1/2,j} \begin{pmatrix} c_x \\ c_x^2 \\ c_x c_z \end{pmatrix} \mathrm{d}t\,\mathrm{d}c_x\,\mathrm{d}c_z \tag{109}$$

Invoking the difference form of the Boltzmann equation (101) leads to the following:

$$\int_{t^n}^{t^{n+1}} \int_{z_{j-1/2}}^{z_{j+1/2}} \mathbf{F}_{i+1/2}\,\mathrm{d}z\,\mathrm{d}t = \alpha\Delta z \int_{-\infty}^{\infty} \int_{-\infty}^{\infty} \bar{h}_{i+1/2,j}^n \begin{pmatrix} c_x \\ c_x^2 \\ c_x c_z \end{pmatrix} \mathrm{d}c_x\,\mathrm{d}c_z$$

$$+ \gamma\Delta z \int_{-\infty}^{\infty} \int_{-\infty}^{\infty} \left[\bar{h}\frac{\partial\bar{\mathbf{\Phi}}}{\partial t}\right]_{i+1/2,j}^n \cdot\mathbf{M} \begin{pmatrix} c_x \\ c_x^2 \\ c_x c_z \end{pmatrix} \mathrm{d}c_x\,\mathrm{d}c_z$$

$$- \tau a\kappa\Delta z \int_{-\infty}^{\infty} \int_{-\infty}^{\infty} \{H(c_x)[h]_{i+1/2-,j}^n + [1-H(c_x)[h]_{i+1/2+,j}^n\} \begin{pmatrix} c_x \\ c_x^2 \\ c_x c_z \end{pmatrix} \mathrm{d}c_x\,\mathrm{d}c_z$$

$$+ \tau a\kappa\Delta z \int_{-\infty}^{\infty} \int_{-\infty}^{\infty} \left\{H(c_x)\left[h\left(c_x\frac{\partial\mathbf{\Phi}}{\partial x} + c_z\frac{\partial\mathbf{\Phi}}{\partial z}\right)\right]_{i+1/2-,j}^n\right\}\cdot\mathbf{M} \begin{pmatrix} c_x \\ c_x^2 \\ c_x c_z \end{pmatrix} \mathrm{d}c_x\,\mathrm{d}c_z$$

$$- \tau a\kappa\Delta z \int_{-\infty}^{\infty} \int_{-\infty}^{\infty} \left\{[1-H(c_x)]\left[h\left(c_x\frac{\partial\mathbf{\Phi}}{\partial x} + c_z\frac{\partial\mathbf{\Phi}}{\partial z}\right)\right]_{i+1/2-,j}^n\right\}\cdot\mathbf{M} \begin{pmatrix} c_x \\ c_x^2 \\ c_x c_z \end{pmatrix} \mathrm{d}c_x\,\mathrm{d}c_z$$

$$+ \tau c\kappa\Delta z \int_{-\infty}^{\infty} \int_{-\infty}^{\infty} c_x H(c_x)[\bar{h}]_{i+1/2,j}^n \left[\frac{\partial\bar{\mathbf{\Phi}}}{\partial x}\right]_{i+1/2-,j}^n \cdot\mathbf{M} \begin{pmatrix} c_x \\ c_x^2 \\ c_x c_z \end{pmatrix} \mathrm{d}c_x\,\mathrm{d}c_z$$

$$-\tau c\kappa\Delta z\int_{-\infty}^{\infty}\int_{-\infty}^{\infty}c_x[1-H(c_x)][\bar{h}]^n_{i+1/2,j}\left[\frac{\partial\bar{\mathbf{\Phi}}}{\partial x}\right]^n_{i+1/2^+,j}\cdot\mathbf{M}\begin{pmatrix}c_x\\c_x^2\\c_xc_z\end{pmatrix}\mathrm{d}c_x\,\mathrm{d}c_z \tag{110}$$

where $\alpha=\Delta t-\tau(1-\mathrm{e}^{-\Delta t/\tau})$, $\gamma=(\Delta t^2/2)-\tau\Delta-\tau^2(1-\mathrm{e}^{-\Delta t/\tau})$ and a, b, d and κ are as defined earlier. The integration of the right-hand side of Equation (110) can be carried out using the identities provided in Appendix B. This completes the evaluation of the x-mass and momentum fluxes (i.e., $\int_{t^n}^{t^{n+1}}\int_{z_{j-1/2}}^{z_{j+1/2}}\mathbf{F}_{i+1/2}\,\mathrm{d}z\,\mathrm{d}t$) for all i. It must be emphasized that all the flux terms on the right-hand side of Equation (110) involve known quantities from time level n. The z-mass and momentum fluxes (i.e., $\int_{t^n}^{t^{n+1}}\int_{x_{i-1/2}}^{x_{i+1/2}}\mathbf{G}_{j+1/2}\,\mathrm{d}z\,\mathrm{d}t$) for all j can be obtained in an analogous manner to that of the x-mass and momentum fluxes.

At this stage, the only remaining unknown on the right-hand side of Equation (108) is $\int_{x_{i-1/2}}^{x_{i+1/2}}\int_{z_{j-1/2}}^{z_{j+1/2}}\int_{t^n}^{t^{n+1}}\mathbf{S}\,\mathrm{d}t\,\mathrm{d}z\,\mathrm{d}x$. Using a first-order approximation, one obtains the following result:

$$\int_{x_{i-1/2}}^{x_{i+1/2}}\int_{z_{j-1/2}}^{z_{j+1/2}}\int_{t^n}^{t^{n+1}}\mathbf{S}\,\mathrm{d}t\,\mathrm{d}z\,\mathrm{d}x=\mathbf{S}^n_{i,j}\,\Delta x\,\Delta z\,\Delta t \tag{111}$$

Of course higher-order approximations could be adopted. This topic will be the subject of later study when we deal with flows where the gravitational and friction terms that comprise $\mathbf{S}$ are the dominant terms in the momentum equations. For the present, however, the main objective is to test the capability of the Boltzmann scheme in resolving complex flow features, such as discontinuities and extreme expansion waves and the interactions of discontinuous and expansion waves. In the vicinity of these flow features, $\mathbf{S}$ is small in comparison with the inertia forces. In fact, comparison of numerical test results with measured data from dam break laboratory experiments in the presence of $\mathbf{S}$ show good agreement (see Figures 8–13).

3.4. Entropy condition

Equation (31) proves that the analytical solution of the Boltzmann equation satisfies the entropy inequality. It is essential to show that the numerical solution of the Boltzmann equation also satisfies the entropy inequality. In fact, this proof has been performed by Xu *et al.* [4]. The result is

$$\sigma\geq-\frac{1}{\tau}\int_0^{\Delta t}\int_{\infty}^{\infty}\int_{\infty}^{\infty}(h-f)\left(\frac{\partial\bar{\mathbf{\Phi}}}{\partial z}\cdot\mathbf{M}t-\frac{\left[\dfrac{\partial\bar{\mathbf{\Phi}}}{\partial z}\cdot\mathbf{M}\right]^2}{2}t^2\right)\mathrm{d}c_x\,\mathrm{d}c_z\,\mathrm{d}t=O(\Delta t)^3\geq 0 \tag{112}$$

Therefore, the Boltzmann scheme produces a unique and physically realizable solution. In fact, the numerical examples section shows that unphysical solutions such as expansion shocks are automatically suppressed.

3.5. Main steps in the computer code

The solution progresses from time level n to the level $n+1$ as follows:

Step 0 From the previous time step calculation, the vector $\mathbf{W}_{i,j}^n = (y, yu, yv)_{i,j}^n$ is known in each cell center (i, j). This vector is stored for one time step.

Step 1 The x and y slopes of $(y, yu, yv)^n$ within each cell are calculated from Equations (37) and (38).

Step 2 The slopes obtained in Step 1 along with Equation (36) are used to calculate $(y, yu, yv)^n$ at each cell interface.

Step 3 The values of $(\bar{y}, \overline{yu}, \overline{yv})^n$ at each cell interface are calculated using Equations (50)–(54).

Step 4 The values obtained in Step 3 along with Equations (56)–(58) are used to calculate the x and y of slopes $(\bar{y}, \overline{yu}, \overline{yv})^n$ within each cell.

Step 5 The slopes obtained in Steps 1 and along with Equation (106) are used to calculate the time derivative of $(\bar{y}, \overline{yu}, \overline{yv})^n$ at each cell interface.

Step 6 The quantities available from Steps 1–5 along with Equation (110) are used to calculate x-mass and momentum flux at all cell interfaces that are orthogonal to x. The z-mass and momentum flux at all cell interfaces that are orthogonal to z are calculated in an analogous manner.

Step 7 The slope $\mathbf{S}_0$ is given from the geometry of the channel bottom. The slope $\mathbf{S}_f$ is obtained by inserting $(y, yu, yv)_{i,j}^n$ into the Manning equation, where the Manning coefficient is given.

Step 8 The values from Step 8 along with Equation (111) are used to calculate the integral of the external forces from n to $n+1$.

Step 9 The quantities available from Steps 0, 6, and 8 along with Equation (108) are used to calculate the solution vector $\mathbf{W}_{i,j}^{n+1}$.

4. NUMERICAL DEMONSTRATION AND DISCUSSION

In this section, the Boltzmann based numerical model is shown to accurately solve open channel flow problems, including (i) strong shock waves; (ii) extreme expansion waves; (iii) a combination of strong shock waves and extreme expansion waves, and (iv) one- and two-dimensional dam break waves. The comparison between the numerical and analytical solutions (or measured data) is based on the L_1^n error of the depth, which is defined at any time t^n as follows:

$$L_1^n = \frac{1}{N_x N_z} \sum_{i=1}^{N_x} \sum_{j=1}^{N_z} \left(\frac{|(y_{i,j}^n)_{\text{numerical}} - (y_{i,j}^n)_{\text{analytical}}|}{(y_i)_{\text{analytical}}} \right) \tag{113}$$

where N_x is the number of grid points in the x-direction and N_z is the number of grid points in the z-direction. When the analytical solution is not available, the 'exact' numerical solution can be used to judge the accuracy of the solution. The 'exact' numerical solution is obtainable

by systematically reducing the grid size until the solution ceases to change (i.e., converges). In cases where experimental results are available, the $y_{\text{experimental}}$ can be submitted for $y_{\text{analytical}}$ in Equation (113).

Note the grid size, Courant number, Manning coefficient, and channel slope used in each example are indicated in the relevant figures and thus will not be repeated in the text. In addition, this paper uses Manning's formula to compute the bed friction resistance.

4.1. The strong shock problem

To test the resolution capability of the Boltzmann based model in modeling discontinuous surfaces, the convergent flow in a rectangular frictionless channel with a length of 400 m and infinite width is modeled. The initial condition is as follows:

$$y = 1.0 \text{ m}, v = 4.0 \text{ m s}^{-1}, x \leq 200 \text{ m}; \text{ and } y = 1.0, v = -4.0 \text{ m s}^{-1}, x \geq 200 \text{ m}$$

The upstream and downstream boundary conditions are: $y(0, t) = y(0, 0)$; $y(L, t) = y(L, 0)$; $yu(0, t) = yu(0, 0)$; $yu(L, t) = yu(L, 0)$, where L is length of the computational domain. L is chosen long enough so that the undisturbed conditions remain valid at $x = 0$ and $x = L$. To avoid repetition, it suffices to state that the same boundary conditions will be utilized in (i) the extreme expansion wave problem, (ii) the one-dimensional dam break problem, (iii) the multistage problem, and (iv) the two-dimensional dam break problem.

The results of the simulation as well as the analytical solution at $t = 40$ s are shown in Figure 2. The figure shows that the proposed model accurately reproduces shock wave fronts. The L_1^n error norm is only 0.13 per cent for Courant number of 0.6.

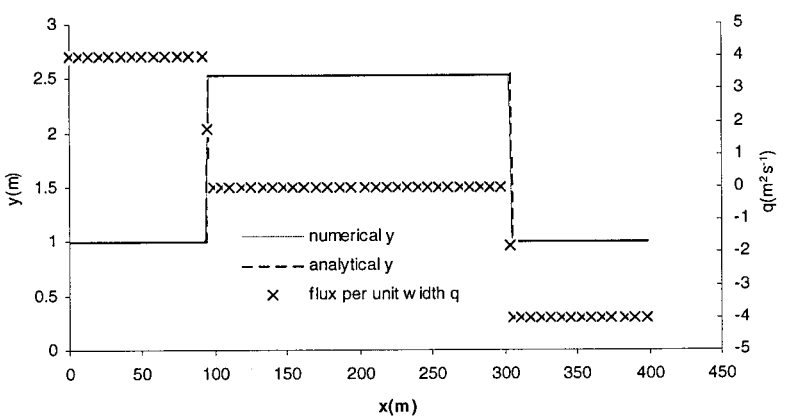

Figure 2. Water depth and flux per unit width for the strong shock wave problem ($\Delta x = 1.0$ m, $C_r = 0.6$, $t = 40$ s, $\mathbf{S}_f = 0.0$, $\mathbf{S}_0 = 0.0$).

4.2. The extreme expansion wave problem

This example tests the accuracy of the Boltzmann model in modeling smooth water profiles. The divergent flow in a rectangular frictionless channel with a length of 300 m and infinite width is modeled. The following initial condition is considered:

$$y = 1.0 \text{ m}, v = -2.0 \text{ m s}^{-1}, x \leq 150 \text{ m}; \text{ and } y = 1.0 \text{ m}, v = 2.0 \text{ m s}^{-1}, x \geq 150 \text{ m}$$

In gas dynamics, this problem is called the Sjögreen problem [20]. The results of the simulation and the exact solution at $t = 20$ s with a Courant number of 0.6 are shown in Figure 3. The figure shows that the proposed model produces results that are highly accurate with the L_1^n error being 0.3 per cent.

4.3. The combination of expansion waves and shocks

One-dimensional dam break problems and the multistage problem are used to test the accuracy of the proposed model in modeling problems containing simultaneously severe shocks and extreme expansion waves.

4.3.1. The one-dimensional dam break problem. The dam break flow in a rectangular frictionless channel with a length of 2000 m and infinite width is modeled. The dam is located at $x = 1000$ m. The severity of the shock and expansion waves in a dam break problem is dependent on the ratio of the initial water depth downstream of the dam to the initial water depth upstream of the dam (R). In the sample cases, R values of 0.5, 0.05, and 0.005 are employed. In addition, to test the influence of Courant number on the accuracy of the scheme, discretization with Courant numbers of 0.1, 0.6, and 0.9 are used respectively. The results of these test cases are shown in Figures 4 and 5. It is clear from these figures that the numerical results are very close to the analytical solution for all depth ratios and all Courant numbers. In addition, all the L_1^n

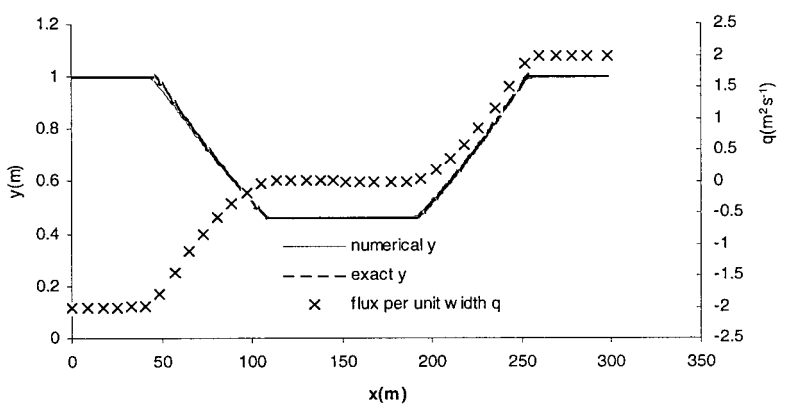

Figure 3. Water depth and flux per unit width for the extreme expansion wave problem ($\Delta x = 1.0$ m, $C_r = 0.6$, $t = 20$ s, $\mathbf{S}_f = 0.0$, $\mathbf{S}_0 = 0.0$).

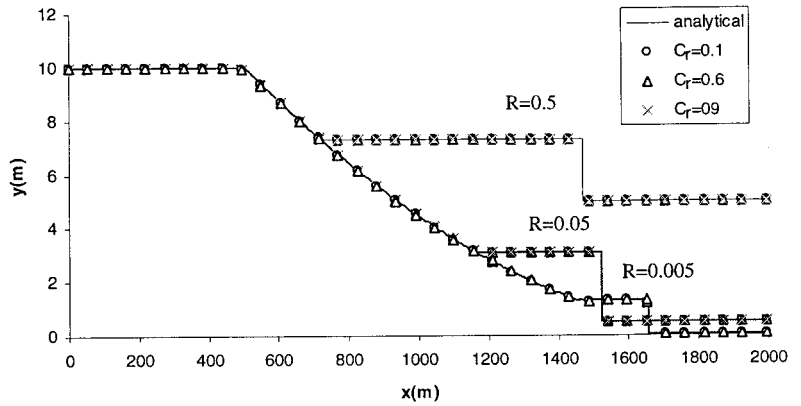

Figure 4. One-dimensional dam-break problem modeling for different values of R and Courant number ($\Delta x = 1.0$ m, $t = 50$ s, $\mathbf{S}_f = 0.0$, $\mathbf{S}_0 = 0.0$).

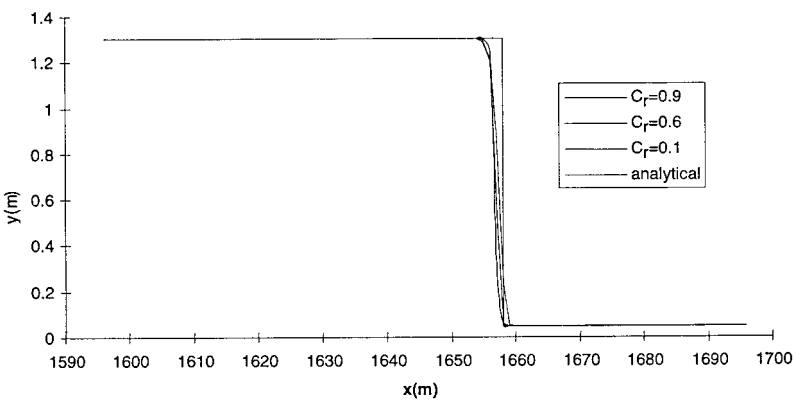

Figure 5. One-dimensional dam-break problem modeling: shock resolution for different values of Courant number ($\Delta x = 1.0$ m, $t = 50$ s, $\mathbf{S}_f = 0.0$, $\mathbf{S}_0 = 0.0$).

error norms are less than 0.4 per cent. Furthermore, Figure 5 shows that the shock resolution is quite insensitive to the Courant number and the shock front is spread over about $3\Delta x$, which is very little smearing. Recall that Nyquist's theorem states that a gird of size Δx cannot resolve a structure smaller than $2\Delta x$.

In is important to ensure that the BGK scheme correctly models energy losses at jumps and bores. The energy loss at a bore is $(y_2 - y_1)^3/4y_1y_2$, where y_1 and y_2 are the water depth upstream and downstream of the bore respectively. Referring to the results in Figure 4 for $R = 0.05$, the energy loss based on the analytic solution is 2.8456 m and the energy loss based on the numerical solution is 2.8367 m (i.e., an error of 0.3 per cent). In addition, referring to

the results in Figure 4 for $R = 0.005$, the energy loss based on the analytical solution is 7.5656 m and the energy loss based on the numerical solution is 7.5120 m, so that the error is 0.7 per cent.

4.3.2. Multistage problem. The Boltzmann procedure was also tested on the more complex flow profile of a multistage problem. The case studied was used by Yang *et al.* [35] to compare the accuracy of shock-capturing finite difference and finite element schemes. The multistage problem is complex in the sense that its solution consists of multiple shock waves, multiple expansion waves and their interaction as well as merging of shock and expansion waves. The computational domain consists of a frictionless, infinitely wide, 500-m long channel. The initial condition of the multistage problem is as follows:

$$y = 100.0 \text{ m},\ v = 0.0 \text{ m s}^{-1} \text{ at } t = 0 \text{ and } x \leq x \leq 250 \text{ m}$$

$$y = 1.0 \text{ m},\ v = 0.0 \text{ m s}^{-1} \text{ at } t = 0 \text{ and } 250 \text{ m} \leq x \leq 350 \text{ m}$$

$$y = 10.0 \text{ m},\ v = 0.0 \text{ m s}^{-1} \text{ at } t = 0 \text{ and } x \geq 350 \text{ m}$$

A Courant number of 0.6 is used. The simulation results at $t = 1$ s (i.e., before the interaction of the shock waves) and $t = 5$ s (i.e., after the shock waves have interacted) are shown in Figure 6. In addition, the numerical and near-exact solutions (obtained by refined steps) at $t = 5$ s are given in Figure 7. The results show that the multiple shocks and expansion waves are well resolved and the proposed model is capable of modeling complex interaction of shock waves. The L_1^n error norm for this example is 0.3 per cent.

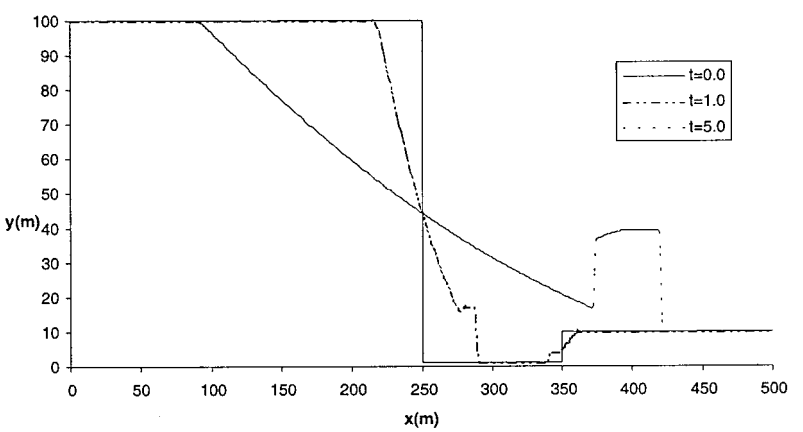

Figure 6. Multistage modeling at $t = 0$, 1, and 5 s ($\Delta x = 1.0$ m, $C_r = 0.6$, $\mathbf{S}_f = 0.0$, $\mathbf{S}_0 = 0.0$).

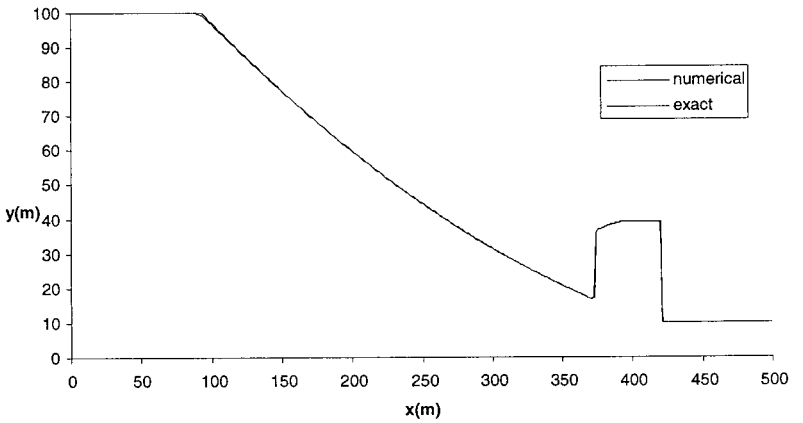

Figure 7. Multistage modeling at $t = 5.0$ s ($\Delta x = 1.0$ m, $C_r = 0.6$, $\mathbf{S}_f = 0.0$, $\mathbf{S}_0 = 0.0$).

4.4. Comparison with measured data

The objective of this example is to compare the numerical results of the proposed BGK model with measured data from dam break laboratory experiments, which were carried by Soulis [36]. These experiments were performed in a rectangular wooden flume lined with plastic-coated plywood, 122 m wide, with a bottom slope of 0.005. The model dam was placed at mid-section, impounding water to a depth of 0.3048 m. In addition, the experiments were carried out using smooth (i.e., $n = 0.009$) and rough (i.e., $n = 0.05$), where n is Manning's coefficient.

The numerical results are generated by the proposed BGK model, where the friction force is represented by Manning's formula. The initial conditions upstream of the dam (i.e., $x \leq 0$) are as follows:

$$y(x, t = 0) = 0.3048 + 0.005x \quad \text{and} \quad u(x, t = 0) = 0 \tag{114}$$

where the units of both x and y is meters and x is the distance along the channel measured from the dam site. The initial conditions downstream of the dam (i.e., $x > 0$) are as follows:

$$y(x, t = 0) = 0.001 \text{ m} \quad \text{and} \quad u(x, t = 0) = 0 \text{ m s}^{-1} \tag{115}$$

In reality, for $x > 0$ the water height $y(x, t = 0) = 0.00$ and not $y(x, t = 0) = 0.01$. However, it is well known that the true dry bed conditions are difficult to treat numerically because of the infinite tangent to the depth profile. Therefore, the small value of 0.001 m is adopted in the calculations. In the calculation, the upstream boundary conditions are: flow velocities are set to zero; water depths are determined by $\partial y/\partial x = 0$. In addition, the downstream-end boundary conditions are: flow velocities are determined by $\partial u/\partial x = 0$; water depths are determined by $\partial y/\partial x = 0$. The computational grid size is $\Delta x = 0.762$ m. Stable results are achieved for all time steps satisfying $C_r \leq 0.6$. For $C_r > 0.6$, numerical instabilities were observed. This reduction in the stability domain is due to the explicit integration of the friction term.

For the smooth case ($n = 0.009$) comparisons of computed water depths with experiments at three different stations, namely $x = -30.5$, 0.0, and 24.4 m, are shown in Figures 8–10. In addition, Figures 11–13 show comparisons for the high friction case (i.e., $n = 0.05$) at $z = -30.5$, 0.0, and 24.4 m. Comparison of numerical test results with measured data from dam break laboratory experiments show good agreement. In addition, the location and time of the bore front is well modeled by the BGK scheme (see Figure 10).

4.5. The two-dimensional dam break problem

Some numerical modeling results of the two-dimensional dam break problem have been reported [37–40]. To test the capability of the present scheme to resolve two-dimensional shock waves, a two-dimensional non-symmetric dam break problem, which is exactly the same

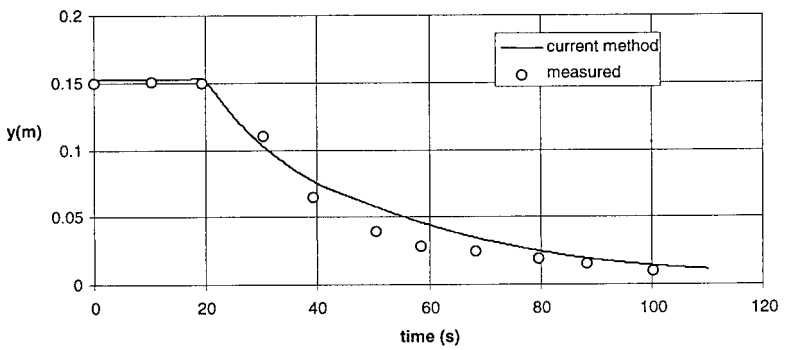

Figure 8. Comparison with measured results at $x = -30.5$ m ($\mathbf{S}_0 = 0.005$, $n = 0.009$, $C_r = 0.6$, $\Delta x = 0.762$ m).

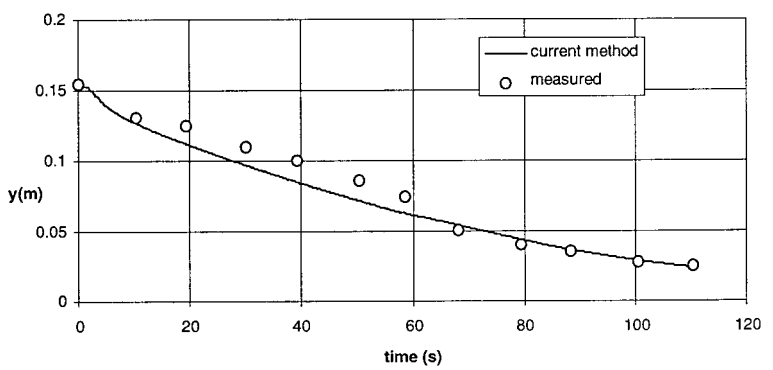

Figure 9. Comparison with measured results at $x = -0.0$ m ($\mathbf{S}_0 = 0.005$, $n = 0.009$, $C_r = 0.6$, $\Delta x = 0.762$ m).

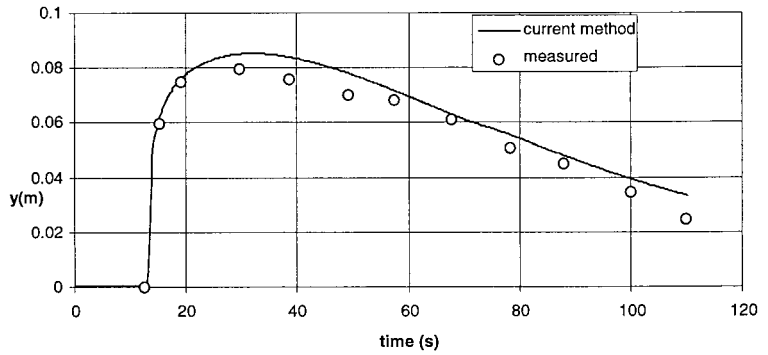

Figure 10. Comparison with measured results at $x = 24.4$ m ($\mathbf{S}_0 = 0.005$, $n = 0.009$, $C_r = 0.6$, $\Delta x = 0.762$ m).

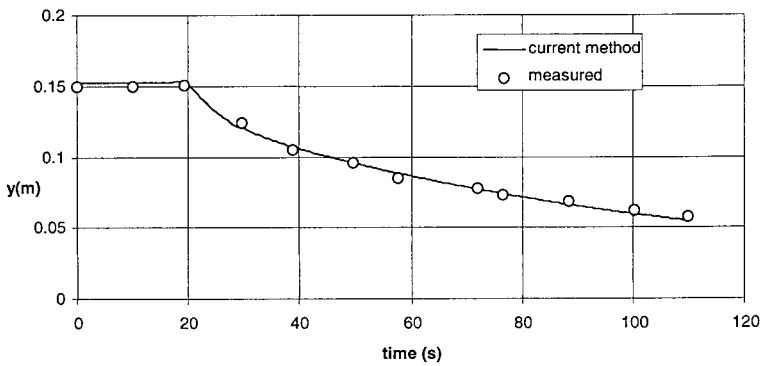

Figure 11. Comparison with measured results at $x = -30.5$ m ($\mathbf{S}_0 = 0.005$, $n = 0.05$, $C_r = 0.2$, $\Delta x = 0.762$ m).

as that used by Fenemma and Chaudhary [38], is used. The computational domain is $(x, z) \in [0, 200 \text{ m}]$. The breach of the dam is 75 m wide and initial water surface is $y(t = 0, x, z) = 10$ m, when $x \leq 100$ and 5.0 m and when $x > 100$ m. The upstream and downstream boundaries are undisturbed. The computational results for time 7.2 s after the dam failure is shown by the three-dimensional plot in Figure 14. This figure shows that the numerical solution is stable and the shock front is well resolved. Figure 15 plots the contour of the water depth. Both the steep gradient in the three-dimensional plot and the high density of the contour lines in the two-dimensional plot highlights the capability of the present model to resolve two-dimensional shock waves.

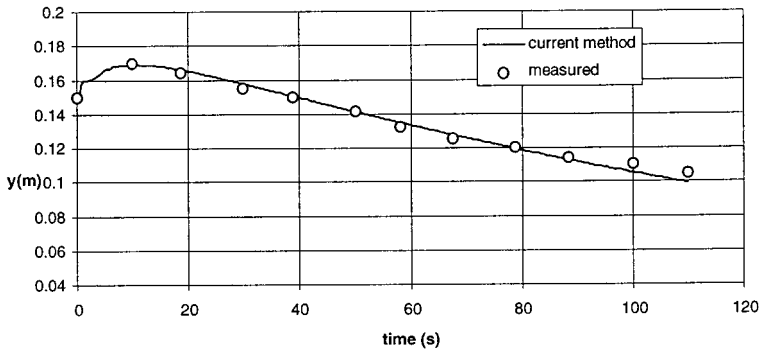

Figure 12. Comparison with measured results at $x = 0.0$ m ($\mathbf{S}_0 = 0.005$, $n = 0.05$, $C_r = 0.2$, $\Delta x = 0.762$ m).

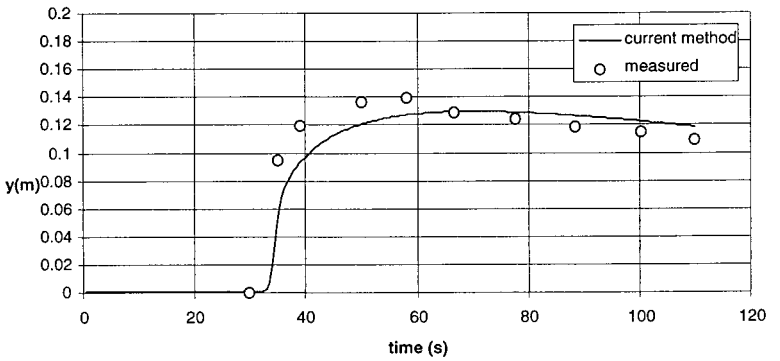

Figure 13. Comparison with measured results at $x = 24.4$ m ($\mathbf{S}_0 = 0.005$, $n = 0.05$, $C_r = 0.2$, $\Delta x = 0.762$ m).

4.6. Remarks on expansion shocks and their absence from the current computation

It is important to emphasize that no entropy fix or artificial diffusion has been added to the present numerical model. Yet none of the computational examples admit unphysical shocks (i.e., expansion shocks). This is expected as Equation (112) shows that the Boltzmann based numerical model satisfies the entropy inequality. On the other hand, solutions based solely on the shallow water equations without consideration of an entropy condition are prone to the development of expansion shocks, unless a carefully designed numerical entropy fix term is added [28,30,41]. However, these entropy fixes lack physical basis and thus may not always be successful [21,42]. For example, Jha *et al.* [42] found that the entropy fix suggested by Alcrudo *et al.* [41] could not avoid the problem of expansion waves. In this regard, Jha *et al.* [42, p. 881] wrote:

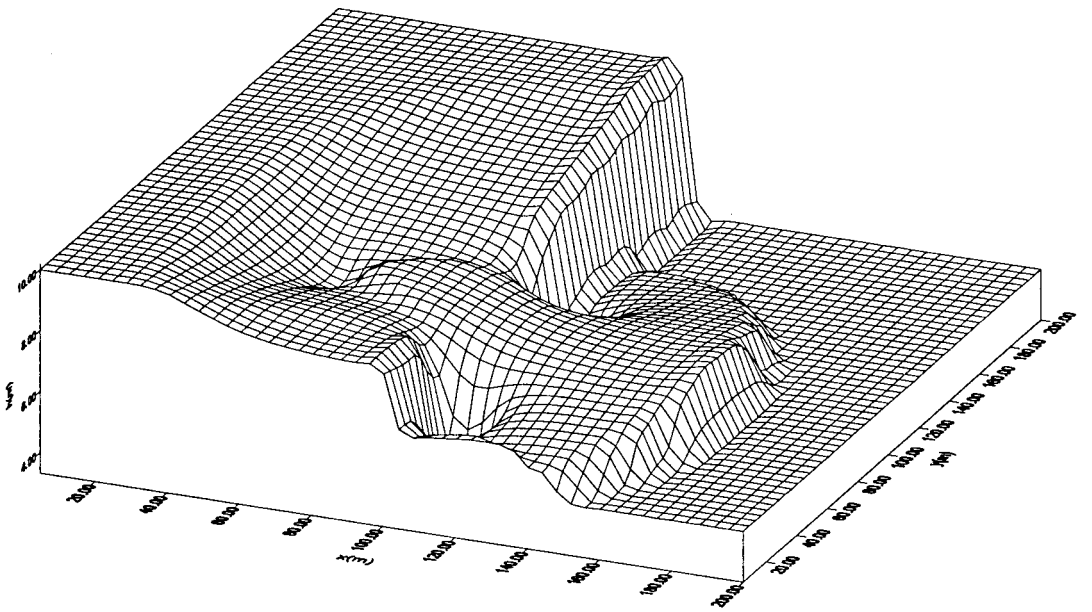

Figure 14. Surface plot of two-dimensional non-symmetric dam-break problem modeling ($\Delta x = \Delta z = 1.0$ m, $C_r = 0.8$, $t = 7.1$ s, $\mathbf{S}_f = 0.0$, $\mathbf{S}_0 = 0.0$).

> These vertical drops in the water-surface profile are due to violation of the entropy-inequality condition, which is obviously not remedied by using a constant value of δ . . . as suggested by Alcrudo *et al.* [41].

Note in the dam break computation the expansion shock usually manifests itself as a vertical drop in the water-surface profile at the location of the dam.

Expansion shocks are difficult to avoid and have been observed in a number of papers. For example, an expansion shock appeared in (i) the McCormack scheme solution (see figures 1-c and 1-d in Reference [41]), (ii) the Osher scheme solution (see figure 3 in Reference [43]), (iii) the Roe scheme solution (see figures 4 and 5 in Reference [42]), and (iv) the flux difference splitting (FDS) scheme solution (see figure 3 in Reference [44]). Therefore, the fact that the current scheme prevents the formation of expansion shocks in itself a useful result.

5. CONCLUSIONS

A finite volume BGK model for one- and two-dimensional unsteady open channel flows has been derived. The proposed model is found to have several advantages. First, the fact that the advective operator in the BGK model is linear helps avoid complex Jacobian matrix computation. Second, the scalar character of the Boltzmann distribution function means that the BGK

model is easily extended to multidimensional flows. Third, the collision function in the Boltzmann equation ensures that the BGK model satisfies the entropy condition and thus prevents the formation of unphysical shocks in open channel solutions.

The BGK scheme was applied to a range of problems with complex features such as strong shock waves, extreme expansion waves, interactions between strong shock waves and extreme expansion waves, and one- and two-dimensional dam break waves. Comparisons with analytical and fine discretization solutions confirm the high accuracy as well as the robustness of the BGK scheme. All the computational results are free of spurious oscillations and unphysical shocks (i.e., expansion shocks). The stability requirement of the BGK scheme when friction is zero is $C_r \leq 1$. Comparison of numerical test results with measured data from dam break laboratory experiments show good agreement. When friction is present, stable results are achieved for $C_r \leq 0.6$. For $C_r > 0.6$, numerical instabilities were observed. This reduction in the stability domain is due to the explicit integration of the friction term.

Although BGK schemes are very promising, they are still in the developmental stage. More research is required to explore the viability of BGK type models for more complex engineering problems encountered in hydraulics and environmental fluid mechanics.

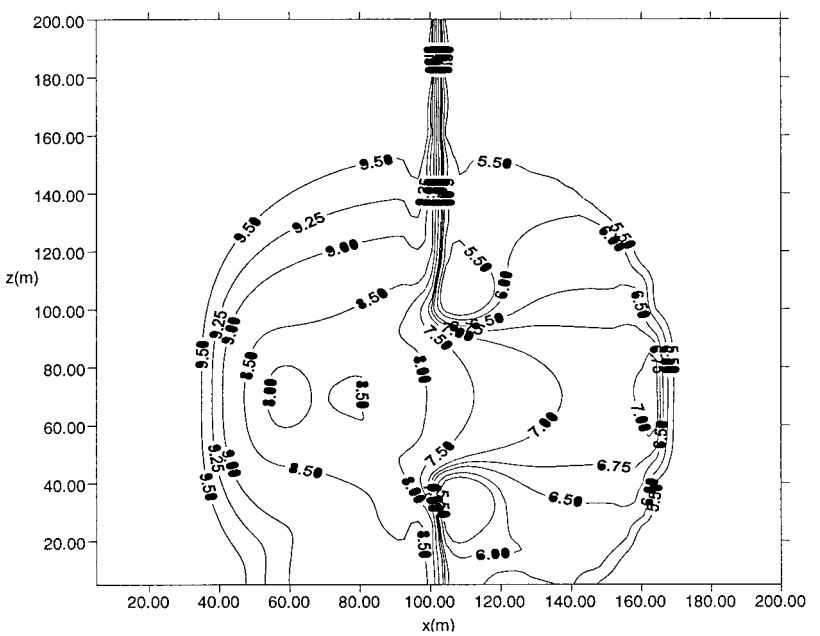

Figure 15. Contour plot of two-dimensional non-symmetric dam-break problem modeling ($\Delta x = \Delta z =$ 1.0 m, $C_r = 0.8$, $t = 7.1$ s, $\mathbf{S}_f = 0.0$, $\mathbf{S}_0 = 0.0$).

ACKNOWLEDGMENTS

The financial support of this work by the Research Grants Council (RGC) of Hong Kong under project number HKUST718/96E is gratefully acknowledged. Additionally, the support for W.G. Gray, provided by the Gledden Fellowship at the University of Western Australia, is gratefully acknowledged.

APPENDIX A. NOMENCLATURE

A	normalizing coefficient
$\mathbf{c}$	particle velocity vector
c_x, c_z	particle velocity in x- and z-directions respectively
C_r	Courant number
erfc	complementary error function
f	non-equilibrium particle distribution function
$\mathbf{F}$	the mass and momentum fluxes along the x-direction
$\mathbf{F}$	external force components acting on particles
g	acceleration due to gravity
$\mathbf{G}$	the mass and momentum fluxes along the z-direction
h	local equilibrium particle distribution function
$\bar{h}$	unique interface equilibrium particle distribution function
H	negative value of entropy
$H(\,.\,)$	Heaviside function
i, j	integer denoting spatial cell location
L	total channel length
L_1	norm error
m	particle mass
$\mathbf{M}$	$=(1, c_x, c_z, c_x^2 + c_z^2)^T$
n	integer denoting time nodal location
p	the depth (area) average water pressure
R	the ratio of the initial water depth downstream of the dam to the initial water depth
S	extensive entropy property
$\mathbf{S}_0$	slope vector of the channel
$\mathbf{S}_\mathrm{f}$	friction slope vector of the channel
t, t^n	time, time at $n\Delta t$
T	transpose
u, v	macroscopic velocities of the fluid in x- and z-directions respectively
$\mathbf{v}$	macroscopic fluid velocity vector
Δt	time step
W	vector whose components are water depth and flow rate, i.e., $(y, yu, yv)^T$
(x, z)	space co-ordinates
X, Z	motion paths of particles
$(\Delta x, \Delta z)$	spatial grid size
y	flow depth of flow

Greek letters

β, γ	dummy variables
δ	variation operator
κ	Boltzmann constant
λ_{0-5}	Lagrange multipliers
ν	viscosity
ρ	density of the fluid
σ	entropy production
τ	relaxation time
τ_{xz}	shear stress at face z along z
$\mathbf{\Phi}$	$=\left(-\dfrac{u^2+v^2}{gy}, \dfrac{2u}{gy}, \dfrac{2v}{gy}, -\dfrac{1}{gy}\right)$

APPENDIX B. USEFUL RELATIONSHIPS

The matrices in Equation (106) are given as follows:

$$[\bar{\Gamma}]^n_{i+1/2,j} = \int_{\infty}^{\infty}\int_{-\infty}^{\infty} \bar{h}^n_{i+1/2,j}\mathbf{MM}\,\mathrm{d}c_x\,\mathrm{d}c_z \tag{116}$$

$$[\bar{\Gamma}^+_{c_x}]^n_{i+1/2,j} = \int_{-\infty}^{\infty}\int_{0}^{\infty} \bar{h}^n_{i+1/2,j}\mathbf{MM}\,\mathrm{d}c_x\,\mathrm{d}c_z \tag{117}$$

$$[\bar{\Gamma}^-_{c_x}]^n_{i+1/2,j} = \int_{-\infty}^{\infty}\int_{-\infty}^{0} \bar{h}^n_{i+1/2,j}\mathbf{MM}\,\mathrm{d}c_x\,\mathrm{d}c_z \tag{118}$$

$$[\Gamma^-_{c_x}]^n_{i+1/2^+,j} = \int_{-\infty}^{\infty}\int_{-\infty}^{0} h^n_{i+1/2^+,j}\mathbf{MM}\,\mathrm{d}c_x\,\mathrm{d}c_z \tag{119}$$

$$[\Gamma^+_{c_x}]^n_{i+1/2^-,j} = \int_{-\infty}^{\infty}\int_{0}^{\infty} h^n_{i+1/2^-,j}\mathbf{MM}\,\mathrm{d}c_x\,\mathrm{d}c_z \tag{120}$$

$$[\bar{\Upsilon}]^n_{i+1/2,j} = \int_{-\infty}^{\infty}\int_{-\infty}^{\infty} \bar{h}^n_{i+1/2,j}c_z\mathbf{MM}\,\mathrm{d}c_x\,\mathrm{d}c_z \tag{121}$$

$$[\bar{\Upsilon}^-_{c_x}]^n_{i+1/2^+,j} = \int_{-\infty}^{\infty}\int_{-\infty}^{0} \bar{h}^n_{i+1/2^+,j}c_z\mathbf{MM}\,\mathrm{d}c_x\,\mathrm{d}c_z \tag{122}$$

$$[\Upsilon^+_{c_x}]^n_{i+1/2^-,j} = \int_{-\infty}^{\infty}\int_{0}^{\infty} h^n_{i+1/2^-,j}c_z\mathbf{MM}\,\mathrm{d}c_x\,\mathrm{d}c_z \tag{123}$$

$$[\bar{\Omega}]^n_{i+1/2,j} = \int_{-\infty}^{\infty}\int_{-\infty}^{\infty} \bar{h}^n_{i+1/2,j} c_x \mathbf{MM}\, \mathrm{d}c_x\, \mathrm{d}c_z \tag{124}$$

$$[\bar{\Omega}^+_{c_x}]^n_{i+1/2,j} = \int_{-\infty}^{\infty}\int_{0}^{\infty} \bar{h}^n_{i+1/2,j} c_x \mathbf{MM}\, \mathrm{d}c_x\, \mathrm{d}c_z \tag{125}$$

$$[\bar{\Omega}^-_{c_x}]^n_{i+1/2,j} = \int_{-\infty}^{\infty}\int_{-\infty}^{0} \bar{h}^n_{i+1/2,j} c_x \mathbf{MM}\, \mathrm{d}c_x\, \mathrm{d}c_z \tag{126}$$

$$[\Omega^-_{c_x}]^n_{i+1/2^+,j} = \int_{-\infty}^{\infty}\int_{-\infty}^{0} h^n_{i+1/2^+,j} c_x \mathbf{MM}\, \mathrm{d}c_x\, \mathrm{d}c_z \tag{127}$$

$$[\Omega^+_{c_x}]^n_{i+1/2^-,j} = \int_{-\infty}^{\infty}\int_{0}^{\infty} h^n_{i+1/2^-,j} c_x \mathbf{MM}\, \mathrm{d}c_x\, \mathrm{d}c_z \tag{128}$$

The evaluation of the right-hand side of the above equations requires knowledge of the various moments of h. These moments are provided below.

B.1. Moments of h at interface $x_{i+1/2}$ for $c_x > 0$

$$[\mu_0]^n_{i+1/2^-,j} = \int_{-\infty}^{\infty}\int_{\infty}^{\infty} h^n_{i+1/2^-,j}\, \mathrm{d}c_x\, \mathrm{d}c_z = \left[\frac{y}{2}\,\mathrm{erfc}\left(-\frac{u}{gy}\right)\right]^n_{i+1/2^-,j} \tag{129}$$

$$[\mu_1]^n_{i+1/2^-,j} = \int_{-\infty}^{\infty}\int_{0}^{\infty} c_x h^n_{i+1/2^-,j}\, \mathrm{d}c_x\, \mathrm{d}c_z = \left[\frac{yu}{2}\,\mathrm{erfc}\left(-\frac{u}{\sqrt{gy}}\right) + \frac{y\sqrt{gy}}{2}\,\mathrm{e}^{-u^2/gy}\right]^n_{i+1/2^-,j} \tag{130}$$

$$[\mu_m]^n_{i+1/2^-,j} = \int_{-\infty}^{\infty}\int_{0}^{\infty} c_x^m h^n_{i+1/2^-,j}\, \mathrm{d}c_x\, \mathrm{d}c_z = [u\mu_{m-1}]^n_{i+1/2^-,j} + \frac{1}{2}\,g(m-1)[y\mu_{m-2}]^n_{i+1/2^-,j}$$
$$\forall m \geq 2 \tag{131}$$

where the subscripts μ_0, μ_1, and μ_m are the zeroth, first and mth moments.

B.2. Moments of h at interface $x_{i+1/2}$ for $c_x < 0$

$$[\mu_0]^n_{i+1/2^+,j} = \int_{-\infty}^{\infty}\int_{-\infty}^{0} h^n_{i+1/2^+,j}\, \mathrm{d}c_x\, \mathrm{d}c_z = \left[\frac{y}{2}\,\mathrm{erfc}\left(\frac{u}{gy}\right)\right]^n_{i+1/2^+,j} \tag{132}$$

$$[\mu_1]^n_{i+1/2^+,j} = \int_{-\infty}^{\infty}\int_{-\infty}^{0} c_x h^n_{i+1/2^+,j}\, \mathrm{d}c_x\, \mathrm{d}c_z = \left[\frac{yu}{2}\,\mathrm{erfc}\left(\frac{u}{\sqrt{gy}}\right) - \frac{y\sqrt{gy}}{2}\,\mathrm{e}^{-u^2/gy}\right]^n_{i+1/2^+,j} \tag{133}$$

$$[\mu_m]^n_{i+1/2^+,j} = \int_{-\infty}^{\infty}\int_{-\infty}^{0} c_x^m h^n_{i+1/2^+,j}\,\mathrm{d}c_x\,\mathrm{d}c_z$$
$$= [u\mu_{m-1}]^n_{i+1/2^+,j} + \frac{1}{2}\,g(m-1)[y\mu_{m-2}]^n_{i+1/2^+,j} \quad \forall m \geq 2 \tag{134}$$

B.3. Moments of h at interface $x_{i+1/2}$ for $-\infty < c_x < \infty$

$$\int_{-\infty}^{\infty}\int_{-\infty}^{\infty} h^n_{i+1/2^+,j}\,\mathrm{d}c_x\,\mathrm{d}c_z = [y]^n_{i+1/2^+,j} \tag{135}$$

$$[E(c_x)]^n_{i+1/2^+,j} = \int_{-\infty}^{\infty}\int_{-\infty}^{\infty} c_x h^n_{i+1/2^+,j}\,\mathrm{d}c_x\,\mathrm{d}c_z = [yu]^n_{i+1/2^+,j} \tag{136}$$

$$[E((c_x-u)^m)]^n_{i+1/2^+,j} = \int_{-\infty}^{\infty}\int_{-\infty}^{\infty} (c_x-u)^m h^n_{i+1/2^+,j}\,\mathrm{d}c_x\,\mathrm{d}c_z$$

$$= \begin{cases} 1\times 3\cdots\times(2p-1)\cdots(m-1)y\left(\sqrt{\dfrac{gy}{2}}\right)^m & \text{if } m \text{ is even} \\ 0 & \text{if } m \text{ is odd} \end{cases} \tag{137}$$

where E is the expected value.

The moments of $\bar{h}$ have analogous forms to those of h. The only difference is that $\bar{y}$ and $\bar{u}$ are used instead of u and y.

It is important to emphasize that, at local equilibrium, c_x and c_z are statistically independent. Therefore

$$\bar{h}(c_x, c_z) = \bar{h}(c_x)\bar{h}(c_z) \quad \text{and} \quad h(c_x, c_z) = h(c_x)h(c_z) \tag{138}$$

This is useful when finding integrals of h and $\bar{h}$ that involve products of c_x and c_z. For example

$$\int_{-\infty}^{\infty}\int_{0}^{\infty} c_z^p c_x^m [h(c_x, c_z)]^n_{i+1/2^-,j}\,\mathrm{d}c_x\,\mathrm{d}c_z = \underbrace{\left(\int_{-\infty}^{\infty} c_z^p h^n_{i+1/2^-,j}\,\mathrm{d}c_z\right)}_{\text{Term A}}\underbrace{\left(\int_{0}^{\infty} c_x^m h^n_{i+1/2^-,j}\,\mathrm{d}c_z\right)}_{\text{Term B}} \tag{139}$$

Terms A and B can be computed from Equations (137) and (131) respectively. In fact, all other moments can be generated from relationships (131), (134), and (137).

APPENDIX C. MASS AND MOMENTUM EQUATIONS

C.1. Consistency of the Boltzmann model with mass balance

The mass balance equation for the two-dimensional open channel flow is obtained by (i) integrating Equation (1) with respect to c_x and c_z from minus infinity to plus infinity, (ii) invoking Equations (3) and (4), (iii) performing integration by noticing Equation (8), and (iv) utilizing the fact that f and $f\mathbf{c}$ have compact support. Note, f, $f\mathbf{c}$ and $f\mathbf{c}\cdot\mathbf{c}$ have compact support because

$$\lim f = 0,\ \lim f\mathbf{c} = 0,\ \text{and}\ \lim f\mathbf{c}\cdot\mathbf{c} = 0 \quad \text{when}\ |\mathbf{c}| \Rightarrow \infty \tag{140}$$

Physically, Equation (140) states that there are zero particles whose velocity magnitude is infinite. If we let $\tau = \epsilon\hat{\tau}$, where ϵ is a small parameter, the result of the integration is

$$\frac{\partial y}{\partial t} + \nabla\cdot(\mathbf{v}y) = \epsilon\hat{\tau}\left\{\frac{\partial}{\partial t}\left[\frac{\partial y}{\partial t} + \nabla\cdot(\mathbf{v}y)\right] + \nabla\cdot\left[\frac{\partial(\mathbf{v}y)}{\partial t} + \nabla\cdot\left(\mathbf{v}\mathbf{v}y + \frac{\partial y}{2}\mathbf{I}\right) - \mathbf{F}y\right]\right\} \tag{141}$$

Both of the terms in brackets on the right-hand side of this equation are $O(\epsilon)$—the first from the self consistency of the present equation, the second as will be shown subsequently in the derivation of the momentum equation. Thus, neglect of these terms is an approximation of second-order smallness that results in mass conservation (32). Equation (141) shows that the Boltzmann model is consistent with the mass balance equation in the two-dimensional unsteady channel flow.

C.2. Consistency of the Boltzmann model with momentum balance

Again, let $\tau = \epsilon\hat{\tau}$, where ϵ is a small dimensionless quantity, expand f as power series in ϵ and substitute the result in Equation (1) to obtain

$$\frac{\mathrm{d}h}{\mathrm{d}t} + \mathbf{F}\cdot\frac{\partial h}{\partial \mathbf{c}} = \frac{h-f}{\tau} + \epsilon\left[\frac{\mathrm{d}}{\mathrm{d}t}\left(\hat{\tau}\frac{\mathrm{d}h}{\mathrm{d}t}\right) + \frac{\mathrm{d}}{\mathrm{d}t}\left(\hat{\tau}\mathbf{F}\cdot\frac{\partial h}{\partial \mathbf{c}}\right) + \mathbf{F}\cdot\frac{\partial}{\partial \mathbf{c}}\left(\hat{\tau}\frac{\mathrm{d}h}{\mathrm{d}t} + \hat{\tau}\mathbf{F}\cdot\frac{\partial h}{\partial \mathbf{c}}\right)\right] + O(\epsilon^2) \tag{142}$$

The momentum equation is obtained by multiplying Equation (142) by $\mathbf{c}$, integrating the result in the particle velocity space, and invoking Equations (9) and (3). The result is

$$\begin{aligned}
&\frac{\partial(\mathbf{v}y)}{\partial t} + \nabla\cdot\left(\mathbf{v}\mathbf{v}y + \frac{\partial y}{2}\mathbf{I}\right) - \mathbf{F}y = \epsilon\hat{\tau}\left\{\nabla\cdot\left(\frac{\partial y^2}{2}\nabla v\right) + \nabla\left[\mathbf{v}\cdot\nabla\left(\frac{\partial y^2}{2}\right)\right] - \nabla\cdot\left[\mathbf{v}\nabla\left(\frac{\partial y^2}{2}\right)\right]\right\} \\
&+ \epsilon\hat{\tau}\left\{\frac{\partial}{\partial t}\left[\frac{\partial(\mathbf{v}y)}{\partial t} + \nabla\cdot\left(\mathbf{v}\mathbf{v}y + \frac{gy}{2}\mathbf{I}\right) - \mathbf{F}y\right] - \mathbf{F}\left[\frac{\partial y}{\partial t} + \nabla\cdot(\mathbf{v}y)\right]\right\} + \epsilon\hat{\tau}\nabla\cdot\left\{\left[\frac{\partial(\mathbf{v}y)}{\partial t}\right.\right. \\
&\left.\left.+ \nabla\cdot\left(\mathbf{v}\mathbf{v}y + \frac{gy}{2}\mathbf{I}\right) - \mathbf{F}y\right]\mathbf{v}\right\} + \epsilon\hat{\tau}\nabla\cdot\left\{y\mathbf{v}\frac{\partial \mathbf{v}}{\partial t} + \mathbf{v}\cdot\nabla\mathbf{v} + g\nabla y - \mathbf{F}\right\}
\end{aligned} \tag{143}$$

where

$$\mathbf{F} = -g(\mathbf{S}_f - \mathbf{S}_0) \tag{144}$$

Note that the last three rows of Equation (143) are all of $O(\epsilon^2)$ in that they involve derivatives of the conservation equations. Thus, these may be neglected in comparison to the left-hand side and the first grouping on the right-hand side to obtain Equation (33). Therefore, the Boltzmann equation provides a second-order accurate approximation to the momentum equation for analysis of open channel flow.

REFERENCES

1. Frisch U, Hasslacher B, Pomeau Y. Lattice gas for the Navier–Stokes equations. *Physical Review Letters* 1986; **56**(14): 1505–1508.
2. Reitz RD. One dimensional compressible gas dynamics calculations using the Boltzmann equations. *Journal of Computational Physics* 1981; **42**: 108–123.
3. Chu CK. Kinetic-theoretic description of the formation of a shock wave. *Physics and Fluids* 1965; **8**: 12.
4. Xu K, Martinelli L, Jamesion A. Gas-kinetic finite volume methods, flux-vector splitting and artificial diffusion. *Journal of Computational Physics* 1995; **120**: 48–65.
5. Xu K, Kim C, Martinelli L, Jameson A. BGK-based schemes for the simulation of compressible flow. *International Journal of Computational Fluid Dynamics* 1996; **7**: 213–235.
6. Gunstension AK, Rothman DH, Zaleski S, Zanetti G. Lattice Boltzmann model of immiscible fluids. *Physics Review A* 1991; **43**(8): 4320–4327.
7. Xu K. BGK-based scheme for multicomponent flow calculations. *Journal of Computational Physics* 1997; **134**: 122–133.
8. He X, Shen X, Doolen GD. Discrete Boltzmann equation model for nonideal gases. *Physics Review* 1998; **57**(1): R13–R16.
9. Rothman DH. Cellular-automation fluids: a model for flow in porous media. *Geophysics* 1988; **53**: 509–518.
10. Chen S, Doolen GD. Lattice Boltzmann method for fluid flows. *Annual Review in Fluid Mechanics* 1998; **30**: 329–364.
11. Chen H, Chen S, Matthaeus WH. Recovery of the Navier–Stokes equations using a lattice-gas Boltzmann method. *Physics Review A* 1992; **45**: R5339–R5342.
12. Martinez DO, Chen S, Matthaeus WH. Lattice Boltzmann magnetohydrodynamics. *Physics of Plasmas* 1994; **1**: 1850–1867.
13. Su M, Xu K, Ghidaoui MS. Low speed flow simulation by the gas-kinetic scheme. *Journal of Computational Physics* 1999; **150**: 17–39.
14. Qian YH. Simulating thermohydrodynamics with lattice BGK models. *Journal of Scientific Computing* 1993; **8**: 321–341.
15. Xu K. A gas-kinetic scheme for the Euler equations with heat transfer. In *Proceedings of the International Symposium on Computational Fluid Dynamics*, Beijing, Zhuang FG (ed.). International Academic Publishers: Beijing, 1997; 247–252.
16. Abbott M, Minns A. *Computational Hydraulics*. Ashgate: Aldershot, 1998.
17. Predergast KH, Xu K. Numerical hydrodynamics from gas-kinetic theory. *Journal of Computational Physics* 1993; **109**: 53–66.
18. Shan X, Doolen G. Multicomponent lattice-Boltzmann model with interparticle interaction. *Journal of Statistics in Physics* 1995; **81**: 379–393.
19. Roberts TW. The behavior of flux difference splitting schemes near slowly moving shock waves. *Journal of Computational Physics* 1990; **90**: 141–160.
20. Einfeldt B, Munz CD, Roe PL, Sjogreen B. On Godunov-type methods near low densities. *Journal of Computational Physics* 1991; **92**: 273–295.
21. Quirk JJ. A contribution to the great Riemann solver debate. *International Journal for Numerical Methods in Fluids* 1994; **18**: 555–574.
22. Senders RH, Prendergast KH. The possible relation of three-kiloparsec arm to explosions in the galactic nucleus. *Astrophysics Journal* 1974; **188**: 489–500.

23. Pullin DI. Direct simulation methods for compressible inviscid ideal gas flow. *Journal of Computational Physics* 1980; **34**: 231–244.
24. Xu K, Prendergast KH. Numerical Navier–Stokes solutions from gas-kinetic theory. *Journal of Computational Physics* 1994; **114**: 9–17.
25. Jou D, Casas-Vazquez J, Lebon G. *Extended Irreversible Thermodynamics*. Springer: Berlin, 1996.
26. Deng JQ, Ghidaoui MS. A numerical scheme for free-surface flow modeling based on kinetic theory. In *Computational Methods in Water Resources XII. Proceedings of XII International Conference on Computational Methods in Water Resources*, Greece, June, vol. 2, Burganos VN, Karatzos GP, Payatakes AC, Brebbia CA, Gray WG, Pinder GF (eds). Computational Mechanics Publications: Southampton, 1998; 411–418.
27. Vincenti GH, Kruger GH Jr. *Introduction to Physical Gas Dynamics*. Krieger Publishing: Malabar, FL, 1965.
28. Lax PD. *Hyperbolic Systems of Conservation Laws and their Mathematical Theory of Shock Waves*. Capital City Press: Montpelier, VT, 1972.
29. Sod GA. *Numerical Methods in Fluid Dynamics*. Cambridge University Press: New York, 1985.
30. LeVeque RJ. *Numerical Methods for Conservation Laws*. Birkhauser: Boston, 1992.
31. Hirsch HT. *Numerical Computation of Internal and External Flows. Volume 2: Computational Methods for Inviscid and Viscous Flows*. Wiley: New York, 1990.
32. van Leer B. Towards ultimate conservative difference scheme V. A second order sequel to Godunov's method. *Journal of Computational Physics* 1977; **32**: 276–299.
33. Abramowitz M, Stegun IA. *Handbook of Mathematical Function with Formulas, Graphs and Mathematical Tables*. Dover Publication: New York, 1972.
34. Hirsch HT. *Numerical Computation of Internal and External Flows. Volume 1: Fundamentals of Numerical Discretization*. Wiley: New York, 1988.
35. Yang JY, Hsu CA, Chang SH. Computations of free surface flows. Part 1: one-dimensional dam-break flow. *Journal of Hydraulic Research* 1993; **31**(1): 19–35.
36. Soulis JV. Computation of two-dimensional dam-break flood flows. *International Journal for Numerical Methods in Fluids*. 1992; **14**: 631–664.
37. Alcrudo F, Garcia-Navarro P. A high-resolution Godunov-type scheme in finite volumes for the 2D shallow water equations. *International Journal for Numerical Methods in Fluids* 1993; **16**: 489–505.
38. Fennel RJ, Chaudhry MH. Explicit methods for 2-D transient free-surface flows. *Journal of Hydraulic Engineering ASCE* 1990; **116**: 1013–1035.
39. Bellos CV, Soulis JV, Sakkas JG. Computation of two-dimensional dam-break-induced flows. *Advances in Water Resources* 1991; **14**: 31–41.
40. Garcia R, Kahawita RA. Numerical solution of the St. Venant equations with the MacCormack finite difference scheme. *International Journal for Numerical Methods in Fluids* 1986; **6**: 259–274.
41. Alcrudo F, Garcia-Navarro P, Saviron JM. Flux difference splitting for 1D open channel flow equations. *International Journal for Numerical Methods in Fluids* 1992; **14**: 1009–1018.
42. Jha AK, Akiyama J, Ura M. First and second order flux difference splitting schemes for dam-break problem. *Journal of Hydraulic Engineering*, *ASCE* 1995; **121**(12): 844–877.
43. Zhao DH, Shen HW, Tabios III GQ, Lai JS, Tan WY. Finite-volume two-dimensional unsteady flow model for river basins. *Journal of Hydraulic Engineering*, *ASCE* 1994; **120**(7): 863–883.
44. Zhao DH, Shen HW, Lai JS, Tabios III GQ. Approximate Riemann solvers in FVM for 2D hydraulic shock wave modeling. *Journal of Hydraulic Engineering* 1996; **122**(12): 669–702.

